Nano Today (2012) 7, 448—466

Available online at www.sciencedirect.com

SciVerse ScienceDirect

journal homepage: www.elsevier.com/locate/nanotoday

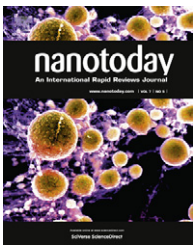

REVIEW

Synthesis and catalytic properties of bimetallic nanomaterials with various architectures

Xiangwen Liu, Dingsheng Wang*, Yadong Li*

Department of Chemistry, Tsinghua University, Beijing 100084, PR China

Received 17 June 2012; received in revised form 25 July 2012; accepted 17 August 2012
Available online 10 September 2012

KEYWORDS
Bimetallic nanomaterials;
Controllable synthesis;
Architectures;
Synergistic effects;
Catalytic properties

Summary Bimetallic nanomaterials have raised more and more significant concern from worldwide researchers in recent years because their new physical and chemical properties derived from synergistic effects between the two metals are highly desirable for specific technological applications, especially for catalytic applications. This review article provides an overview of recent developments in synthesis and properties of bimetallic nanomaterials. First, we summarize recent contributions on developing strategies for the controllable synthesis of bimetallic nanomaterials with various architectures including crown-jewel structure, hollow structure, heterostructure, core—shell structure, alloyed structure and porous structure. Then, we discuss how the microstructural parameters such as surface structure, composition, size, and morphology (crystal facet) influence catalytic properties of bimetallic nanomaterials. Finally, we conclude with our personal perspectives of future research in bimetallic nanomaterials.

Introduction

During the past decade, the design and synthesis of bimetallic nanomaterials have attracted considerable attention, because they show multiple functionalities and prominent catalytic activity, selectivity, and stability over monometallic nanomaterials [1—5]. Bimetallic catalytic systems can potentially achieve chemical transformations that are unprecedented with monometallic catalysts because different components of the catalyst have a particular function in the overall reaction mechanism [6—8]. For example [6], Pd is an effective catalyst for acetoxylation of ethylene to vinyl acetate (VA). Although the VA formation rate on an Au-only surface is negligible, the addition of Au to Pd can greatly enhance Pd's overall catalytic activity, selectivity, and stability. The role of Au is to isolate single Pd sites that facilitate the coupling of critical surface species to product, while inhibiting the formation of undesirable reaction by-products (CO, CO_2, and surface carbon). The experimental results demonstrate that larger ensembles containing contiguous Pd atoms are much less efficient than a properly spaced pair of Pd monomers. Therefore, larger Pd ensembles are not required for acetoxylation of ethylene to VA. Very recently, Sykes and co-workers [8] showed that the Pd/Cu single-atom alloy surface displayed a rather uncommon energetic landscape for the dissociation and chemisorption of hydrogen. Temperature-programmed desorption measurements

* Corresponding authors.
E-mail addresses: wangdingsheng@mail.tsinghua.edu.cn (D. Wang), ydli@mail.tsinghua.edu.cn (Y. Li).

1748-0132/$ — see front matter © 2012 Elsevier Ltd. All rights reserved.
http://dx.doi.org/10.1016/j.nantod.2012.08.003

demonstrated that desorption of H_2 from Cu(1 1 1) occurred at ~310 K and from Pd(1 1 1) at ~320 K. Comparatively, H_2 desorption from Pd/Cu occurred at ~210 K, which was much lower than that expected for H_2 desorption from Cu(1 1 1) or Pd(1 1 1). These data revealed that individual, isolated Pd atoms in a Cu surface substantially lower the energy barrier to both hydrogen uptake on and subsequent desorption from the Cu metal surface, and might be prominent catalysts for selective hydrogenation of styrene and acetylene over pure Cu or Pd metals.

Since bimetallic nanocrystals are composed of two different metal atoms, the atomic distribution can greatly influence the final architectures of nanocrystals, which could have a significant impact on their catalytic performance [9—12]. Taking Au/Pd bimetallic nanocrystals as an example [9], Au—Pd alloy nanocrystals form when there is a uniform distribution between Au and Pd atoms, whereas Au@Pd core—shell nanocrystals form when Au is surrounded by Pd atoms. Many reports have demonstrated that Pd nanostructures have efficient electrocatalytic activity for formic acid oxidation, and incorporation of Au into Pd catalysts can improve catalytic activity and selectivity and provide resistance to poisoning. However, the manner of incorporation will influence the properties of catalysts, that is, the activity and selectivity of Au/Pd bimetallic nanocatalysts can be tuned by changing their atomic distributions. Although Au can't directly oxidize formic acid, it can induce the improvement of the CO oxidation capability through the lowering of CO adsorption energy, leading to the formation of more available Pd active sites for the formic acid oxidation. Because Au on the surface blocks the adsorption of CO more effectively than Au in the core, Au—Pd alloy nanocrystals show higher electrocatalytic activity and stability than Au@Pd core—shell nanocrystals. Besides core—shell and alloyed structures, bimetallic nanocrystals can also form other architectures depending on atomic arrangements. Since there is a close relationship between structures and properties, the rational controlled synthesis of bimetallic nanocrystals is of vital importance for their applications [13—17].

Although significant progress has been made in the controllable synthesis of nanocrystals with well-defined composition, structure, size, and morphology in recent years [18—25], more accurate control over nucleation and growth stages is required to achieve formation of bimetallic nanocrystals [26—30]. Bimetallic nanomaterials can emerge with various architectures including crown-jewel structure, hollow structure, heterostructure, core—shell structure, alloyed structure and porous structure. Different synthetic strategies have been developed to prepare bimetallic nanocrystals with well-defined architectures [31—40]. Actually, in addition to bimetallic nanomaterials, trimetallic and multimetallic nanocrystals have also attracted broad attention from worldwide scientists in recent years. Heterometallic nanocrystals composed of three or more metal elements may possess an even greater degree of catalytic properties due to more tunable variables compared with mono- and bi-metallic nanocrystals. This is a quickly developing field [41—50]. This review article only focuses on bimetallic nanomaterials. For broader discussions on heterometallic nanocrystals, readers are referred to a few excellent review articles, especially Xu's feature article on recent progress in synergistic catalysis over heterometallic nanoparticles [51]. Herein, we first introduce these synthetic methods and discuss how to achieve accurate control over morphology, size, composition, and structure of bimetallic nanocrystals by tuning thermodynamic parameters (temperature, reduction potential, etc.) and kinetic parameters (reactant concentration, diffusion, solubility, reaction rate, etc.). In the second part of the review, our discussions are focused on how microstructural parameters can alter the catalytic properties of bimetallic nanomaterials. We finally present our perspectives on the future directions in this promising field.

Synthesis of bimetallic nanomaterials with various architectures

Crown-jewel structure

Crown-jewel structure means that one metal atom (single atom) is controllably assembled at the special position on the surface of the other metal atoms. Generally, the ''jewel'' metal is the more expensive metal with catalytic activity. There are at least two advantages to construct crown-jewel structure for their catalytic applications. One is the effective use of precious metal atoms. Because the precious metal atoms locate at the surface of the cheaper metals, each precious metal atom can engage in chemical reactions. The other is the improved catalytic performance of the catalyst. Since each precious metal atom is surrounded by several cheaper metal atoms, the adjacent second element can often modify the electronic state of the primary catalytic component and improve their catalytic properties.

It is not an easy task to synthesize bimetallic nanomaterials with crown-jewel structure considering that the control is on an atomic level. The commonly used method is the chemical vapor deposition (CVD) approach, that is, one metal atom is deposited onto another metal surface. Pd/Cu single-atom alloys were prepared via this method by Sykes's group [8]. Pd deposition was performed in ultra high vacuum instrument via electron beam evaporator. The evaporated Pd adatoms adsorb on the substrate and diffuse over the terraces in a random walk fashion until they are trapped at the nearest ascending step edge where place exchange and alloying into the Cu surface layer takes place. Scanning tunneling microscopy (STM) image shows atomically dispersed Pd atoms in a Cu(1 1 1) surface (Fig. 1). The surface concentration of Pd can be tuned by accurate and reproducible control of metal flux.

Bimetallic nanomaterials with crown-jewel structure can also be obtained via solution state method. However, the solution-based process is more difficult to control compared with CVD approach. Toshima and co-workers demonstrated the preparation of crown-jewel-structured Au/Pd nanocluster catalysts by a galvanic replacement reaction method [52]. An aqueous solution of $HAuCl_4{\cdot}4H_2O$ was dropwise added into an as-prepared Pd_{147} colloidal dispersion with continuous stirring at room temperature in a N_2 atmosphere. After heat treatment for 30 min in a bath of 100 °C, Au/Pd with crown-jewel structure formed, in which Pd_{147} nanocrystals serve as the crown, whereas the Au atoms serve as jewels decorating the top position of the Pd_{147} nanocrystals

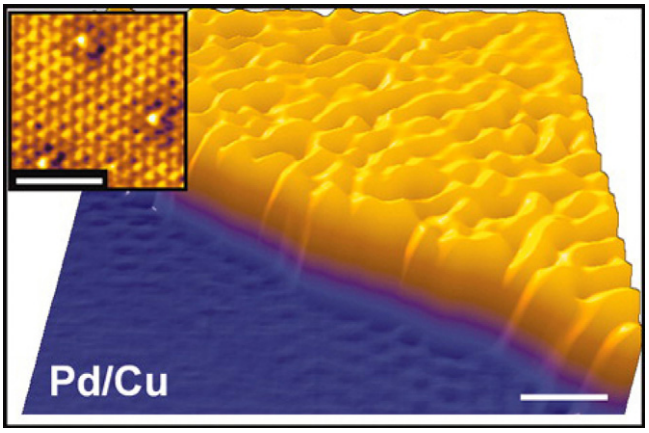

Figure 1 STM image showing atomically dispersed Pd atoms in a Cu(1 1 1) surface (scale bar: 5 nm); inset: atomic resolution of the Pd/Cu alloy (scale bar: 2 nm).
Reproduced with permission from [8].

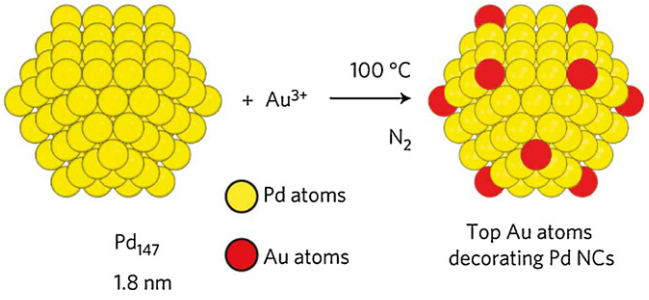

Figure 2 Schematic illustration of producing crown-jewel-structured Au/Pd nanoclusters.
Reproduced with permission from [52].

(Fig. 2). To achieve this replacement reaction, it is critical to strictly control the concentration of Au precursors and the reaction conditions. Because the replacement reaction on the surface of the Pd_{147} nanocrystals first occurs from the top Pd atoms, the top Pd atoms have a preferential probability to react with the Au^{3+} ions to form in situ the top Au atoms when low concentration of Au precursors are used and the reaction is performed in proper conditions. The ''crown-jewel-structure'' concept potentially provides a general design of bimetallic nanomaterials with a catalytically active metal (noble metal) embedded in catalytically less active metals (cheaper metals).

Hollow structure

Hollow nanostructures have attracted steadily growing attention owing to their unique structure (high surface to volume ratio and large pore volume) that can be useful in realizing multifunctional materials [22—24]. On one hand, their interior void can not only serve as an extremely small container for encapsulating multifunctional active materials, but also be used as a reaction chamber or a ''nano-reactor''. On the other hand, their shell structure (thickness, porosity, and surface derivatization) can be well modified to meet various applications. Recently, the synthesis and applications of hollow nanostructures have been comprehensively reviewed by many groups (e.g. Cheng and Sun [22], An and Hyeon [24], Zhang et al. [23], Lou et al. [53], etc.). However, examples of bimetallic hollow nanostructures are relatively rare. Bimetallic nanomaterials with hollow structure exhibit catalytic activities different from their solid counterparts with the advantages of low density, saving of materials, and reduction of costs. Herein, we review recent progress in synthesis of bimetallic hollow nanostructures.

The most effective approach for generating hollow nanostructures is the template-mediated strategy which includes hard-templating, soft-templating, and sacrificial templating methods [23]. Using pre-prepared metal nanoparticles as the sacrificial template, bimetallic hollow nanostructures of various morphologies can be fabricated via the galvanic replacement reaction which takes place when the metal nanoparticles are in contact with other metal ions of higher reduction potential [54—56]. Very recently, Puntes and co-workers [5] demonstrated successful synthesis of bimetallic hollow nanoparticles via the simultaneous or sequential action of galvanic replacement and the Kirkendall effect. By using silver as template; $HAuCl_4{\cdot}4H_2O$ as oxidizing agent; polyvinylpyrrolidone (PVP) as surfactant; cetyl trimethylammonium bromide (CTAB) as surfactant and complexing agent; and ascorbic acid as reducing agent, AuAg double-walled nanoboxes were produced in a simple manner at room temperature (Fig. 3). This example indicates that, with minor modifications in the chemical environment, it is possible to control the reaction and diffusion processes, opening up a synthetic route for the production of bimetallic hollow nanoparticles.

Although template-mediated approaches are effective and easily controllable methods for preparing a wide array of hollow structures, disadvantages related to high cost and tedious synthetic procedures have impeded scale-up of these methods. Because of this, much effort has been devoted to establishing one-step template-free methods to synthesize hollow nanostructures [57—59]. For example, Yang and co-workers [57] showed the preparation of hollow PdCu alloyed nanocubes by a novel one-pot template-free strategy through tuning the surface energy difference of the crystal planes by alloying. Our group has also made some progress in one-pot synthesis of bimetallic hollow nanostructures including Pt/Cu hollow nanoparticles [58] and Pd/Sn single-crystalline hollow nanospheres [59]. In a typical synthesis of hollow Pd/Sn, $SnCl_2{\cdot}2H_2O$, $Pd(acac)_2$ and didodecyldimethyl-ammonium bromide (DDAB) dissolved in oleylamine (OAm) were added into mixed solvent of octadecene (ODE) and OAm at the same time, hollow bimetallic Pd/Sn nanospheres with an average diameter of 10 nm could be obtained within 15 min. The TEM and high-resolution TEM (HRTEM) images (Fig. 4) reveal that the as-prepared Pd/Sn nanospheres show fine single-crystalline hollow nanostructures with ordered atoms arrangement. The above mentioned progress has made it possible to synthesize bimetallic hollow nanostructures in a cost-effective and high-throughput way.

Heterostructure

Since Xia and co-workers confirmed that the Pd—Pt bimetallic nanodendrites were two and a half times more active

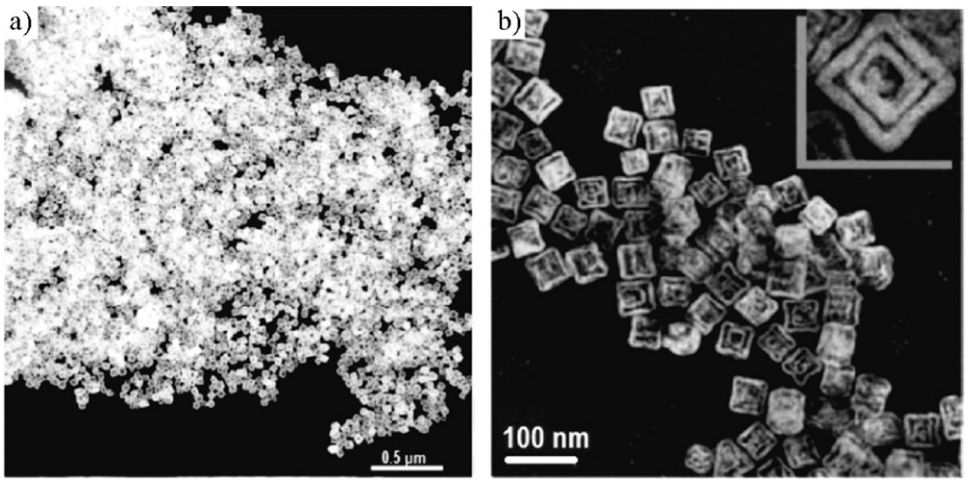

Figure 3 TEM images of AuAg double-walled nanoboxes at different magnifications.
Reproduced with permission from [5].

on the basis of equivalent Pt mass for the oxygen reduction reaction (ORR) than the state-of-the-art Pt/C catalyst and five times more active than the first-generation supportless Pt-black catalyst [3], Pt-based bimetallic heteronanostructures have attracted considerable interest because these materials are urgently desired in proton-exchange membrane fuel cells (PEMFCs) [60—62]. Heterogeneous seeded growth is probably the most powerful route to construct bimetallic heterostructures [63—68]. For example, Pt-on-Pd heterogeneous bimetallic nanostructures have been synthesized by the reduction of $Pt(acac)_2$ in an organic medium (mixture of oleylamine and diphenyl ether) in the presence of Pd nanoparticles as seeds [67]. The Pd—Pt nanodendrites consisting of a dense array of Pt branches on a Pd nanocrystal core were synthesized in an aqueous solution by reducing K_2PtCl_4 with L-ascorbic acid in the presence of 9-nm truncated octahedral Pd seeds, with the addition of PVP as a stabilizer [62]. The ligand-free Pt-on-Au nanodendrites could be obtained when an aliquot of Na_2PtCl_4 was added to an aqueous suspension containing Au@h-SiO_2 nanospheres as seeds and L-ascorbic acid as the reducing agent [60]. Considering that the two-step synthetic methods based on seed-mediated growth are strongly dependent on the use of pre-formed faceted metal seeds to direct the subsequent growth of the Pt branches, Yamauchi and coworkers developed a very simple and high-yield route for the direct synthesis of Pt-on-Pd nanodendrites in aqueous solution without the need for any pre-formed Pd seeds [61]. In their synthesis, an aqueous solution containing K_2PtCl_4, Na_2PdCl_4, and Pluronic P123 was mixed with ascorbic acid which was used as a reducing agent. The final products could be obtained at room temperature within 30 min. Fig. 5a shows TEM image of the as-prepared products which consist of well-dispersed nanodendrites with complete dendritic shape. From the HRTEM image (Fig. 5b), it can be seen that the nanoparticle was a dendritic entity having Pt nanoarms branching in various directions. The EDS mapping images of one nanoparticle (Fig. 5c) confirmed that Pt was distributed

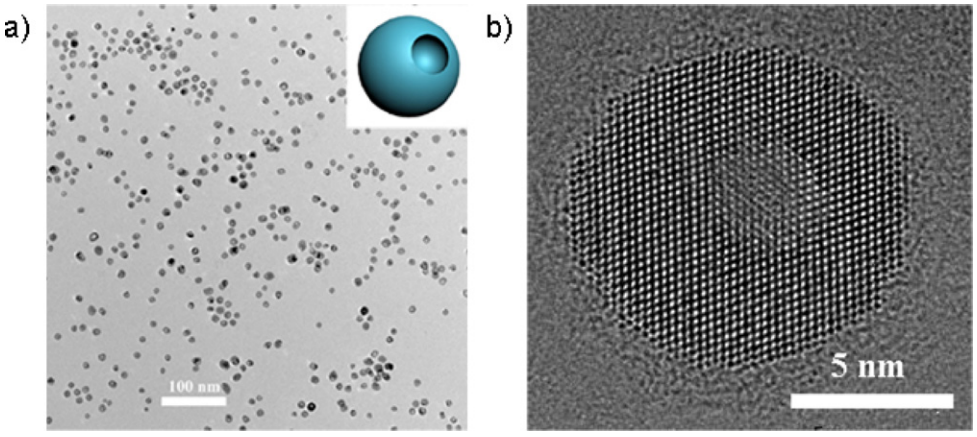

Figure 4 TEM (a) and HRTEM (b) images of Pd/Sn single-crystalline hollow nanospheres.
Reproduced with permission from [59].

throughout the entire nanodendrite and that Pd was concentrated in the core domain.

Besides Pt-based heterostructures, other bimetallic heteronanostructures have also been synthesized, including Pd—Au dimers obtained via Au overgrowth on Pd nanocubes [69], Au—Ag head—body nanosnowman structures obtained via Ag overgrowth on DNA-modified Au nanoparticles [70], and Pd—Ag heterostructures obtained via Ag overgrowth on Pd nanocubes [71]. All of these nanostructures were prepared by seed-mediated growth. In this process, it is a crucial step to control the reaction kinetics which can direct the heterogeneous nucleation and growth on a seed to follow a conformal or site-selective mode. There are many strategies to manipulate the reaction kinetics, such as variation of the reductant, tuning of precursor concentration, or control of the injection rate of precursor. Very recently, Xia and co-workers [71] demonstrated successful preparation of Pd—Ag bimetallic nanocrystals with different structures by simply manipulating the rate at which $AgNO_3$ was added. Pd—Ag dimers were obtained when injecting the Ag precursor at a slow pace (Fig. 6a—c). When $AgNO_3$ was added at a moderate rate, eccentric heterostructure of Pd—Ag (Ag grew on three adjacent faces of a Pd seed) was obtained (Fig. 6d—f). In contrast, when the injection rate is rapid, Pd—Ag core—shell nanoparticles were obtained (Fig. 6g—i). The core—shell structure of bimetallic nanocrystals will be discussed in the following section.

Core—shell structure

As mentioned above, in the seed-mediated growth process, when the heterogeneous nucleation and growth on pre-formed seeds of one metal follow a conformal mode, the second metal will grow on all faces of the seed, leading to the formation of core—shell structure. Bimetallic core—shell nanomaterials, made with an active-metal shell supported on another metal as a core element, are emerging as one of the most promising catalysts with high efficiency [72—76]. Because the catalytic reaction generally takes place only on the surface of the nanoparticles, the interior atoms are often wasted. This is a serious problem especially for noble-metal catalysts due to the high cost and limited reserves of noble-metal materials. From this point, constructing core—shell structure by replacing the interior atoms with cheaper metals might be one of the best solutions to addressing this issue. The core metal can not only reduce active-metal usage, but also markedly affect the performance of the whole nanoparticles.

In general, bimetallic core—shell nanoparticles are prepared by seed-mediated growth or one-pot co-reduction of metallic precursors [77—80]. Actually, the one-pot co-reduction process is similar to seed-mediated growth in nature. When two metallic precursors are added into the synthetic system at the same time, one metal ion will be reduced first due to the difference in the reduction potentials of the two metal cations. The pre-formed metal will serve as in situ seeds for the successive reduction and growth of another metal. So far, bimetallic core—shell nanocrystals with well-defined shapes have been synthesized by many groups [77—82]. For example, Zheng and co-workers reported the synthesis of Pd@Ag core—shell nanoplates via epitaxial growth of Ag on uniform hexagonal Pd nanoplates [77]. Han and co-workers demonstrated the preparation of convex polyhedral Au@Pd core—shell nanocrystals enclosed predominantly by high-index {12 5 3} facets under aqueous room-temperature conditions through simultaneous reduction of Au and Pd ions in the presence of octahedral Au nanocrystal seeds [78]. Wiley and co-workers described the formation of AuPd nanoflowers with Au core and Pd petals through reduction of Pd ions by hydroquinone in the presence of Au nanoparticles and PVP [79]. Very recently, Hwang and co-workers developed a general protocol for the fabrication of well-defined bimetallic core@shell structured nanoparticles via a kinetically controlled autocatalytic chemical process [80]. In their process, a sacrificial Cu ultrathin layer is autocatalytically deposited on a dimensionally stable noble-metal core under kinetically controlled conditions, which is then displaced to form an active ultrathin metal-layered shell by redox-transmetalation (Fig. 7a). Fig. 7b and c show TEM images of Pd@Pt nanocrystals with Pt ultrathin layer on spherical and cubic Pd nanoparticles respectively. The $Pd_{core}Pt_{ultrathin\text{-}shell}$ nanoparticles which maximize the Pt's surface to volume ratio are achieving prominence due to their enhanced catalytic properties and significant economic advantages.

A far more complex class of core—shell nanoparticles concerns multishelled nanostructures [83,84]. To achieve the synthesis of this complex structure, much more precise kinetic control over the reaction is required. Xu and co-workers demonstrated the successful synthesis of Au/Co/Fe nanoparticles which have a triple-layered core—shell structure composed of a Au core, a Co-rich inter-layer, and a Fe-rich shell via a one-step in situ procedure [83]. Xia and co-workers also described the synthesis of multishelled nanocrystals composed of alternating shells of Pd and Pt by starting with seeds made of Pd or Pt nanocrystals through a layer-by-layer epitaxial approach [84]. Fig. 8a schematically shows how multishelled nanocrystals are obtained by alternating the deposition of Pt and Pd shells on a seed of Pd cuboctahedron. Via layer-by-layer epitaxial overgrowth, Pd@Pt (Fig. 8c), Pd@Pt@Pd (Fig. 8d), and Pd@Pt@Pd@Pt (Fig. 8e) nanocrystals can be successfully prepared. Such cases of nanostructures would potentially exhibit new features arising from the effective coupling between adjacent layers.

Alloyed structure

When two distinct metal atoms have a homogeneous distribution in one particle, bimetallic alloys form. In the wet-chemical synthesis of bimetallic nanocrystals, two kinds of metals thermodynamically prefer to nucleate and grow separately because of their different standard reduction potentials, leading to the formation of core—shell or heterostructured particles. In order to produce alloyed nanocrystals, the reaction kinetics must be rigidly controlled. There are several routes to achieve this control [85—88]. One feasible route is to use strong reducing agents that can reduce simultaneously all metal precursors at proper rates. Xu and co-workers demonstrated the successful synthesis of noble-metal-free Ni—Fe alloy nanoparticles by a surfactant-aided co-reduction process [89]. Sodium borohydride was used as strong reducing agent to reduce Ni^{2+} and Fe^{2+} ions in an aqueous solution. The second route

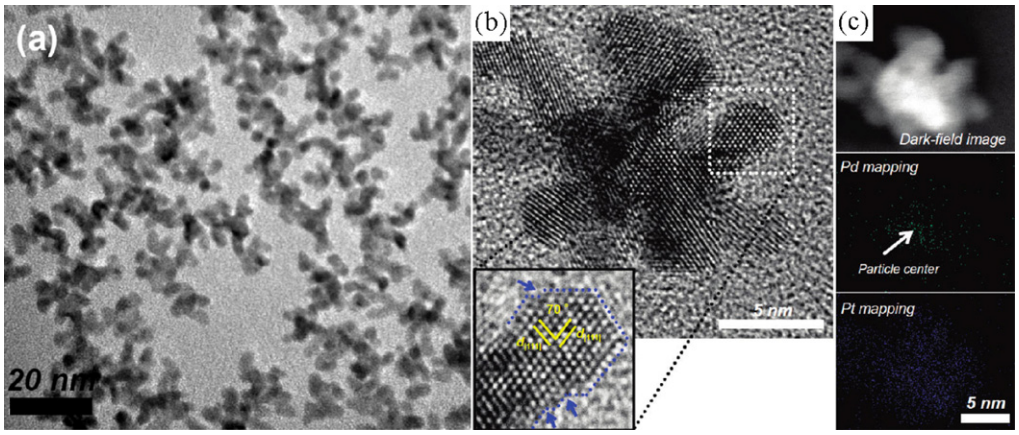

Figure 5 TEM (a), HRTEM (b), and EDS mapping (c) images of Pt-on-Pd nanodendrites.
Reproduced with permission from [61].

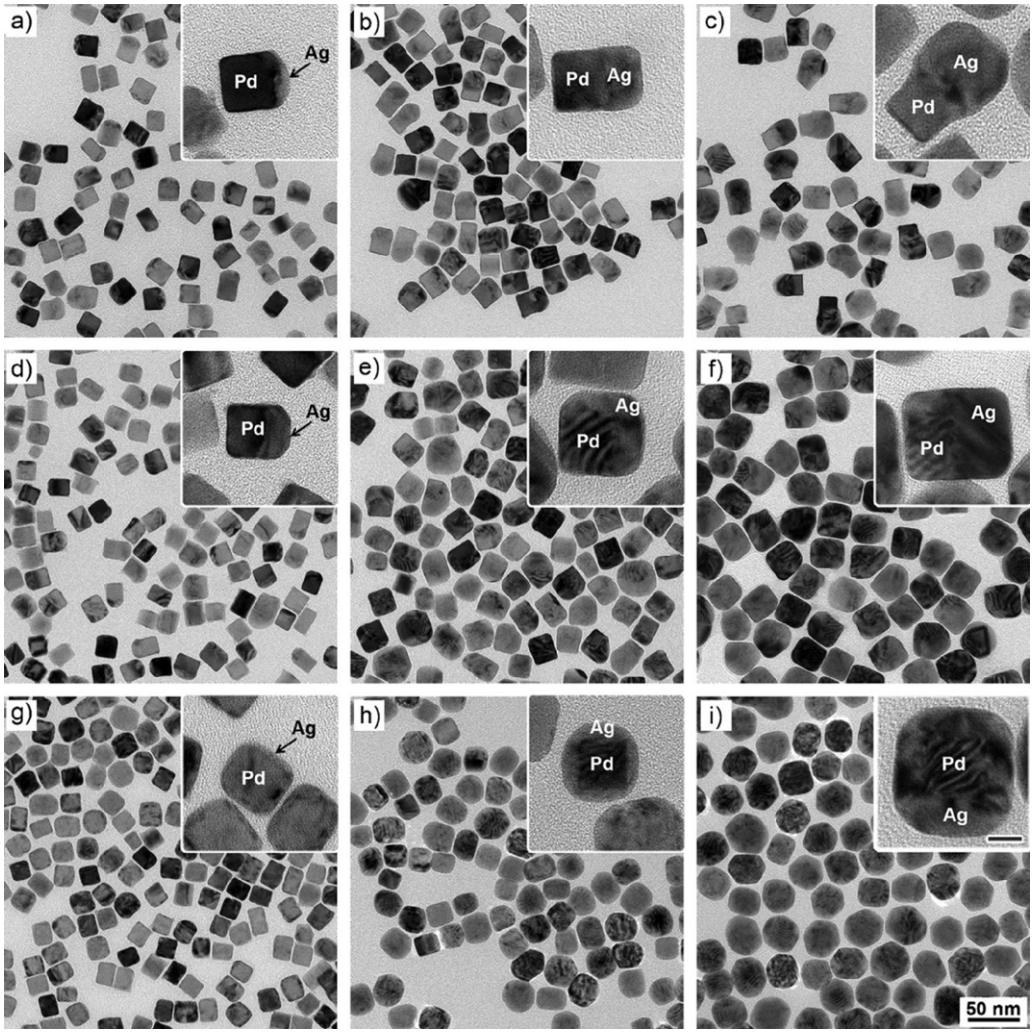

Figure 6 (a–c) TEM images of Pd–Ag dimers obtained with different volumes of added $AgNO_3$ solution; (d–f) TEM images of Pd–Ag eccentric nanobars obtained with different volumes of added $AgNO_3$ solution; (g–i) TEM images of Pd@Ag core–shell nanocrystals obtained with different volumes of added $AgNO_3$ solution. Insets: enlargements, scale 10 nm and applies to all insets; the 50 nm scale bar applies to all main images.
Reproduced with permission from [71].

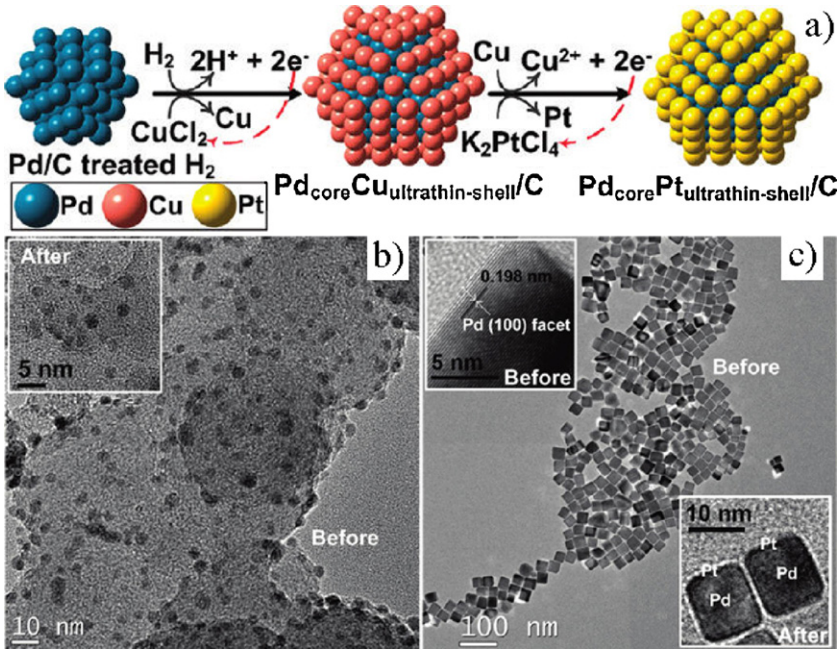

Figure 7 (a) Schematic illustration of producing $Pd_{core}Pt_{ultrathin\text{-}shell}$ nanoparticles; (b—c) TEM images of Pd nanoparticles with different morphologies and corresponding Pd@Pt nanocrystals (insets).
Reproduced with permission from [80].

is to select appropriate surfactant or counterions. Through specific adsorption or coordination, the redox potentials of metals can be adjusted, leading to simultaneous reduction of different metal ions. Han and co-workers proved one-pot synthesis of rhombic dodecahedral Au—Pd alloyed nanocrystals via co-reduction of $HAuCl_4$ and K_2PdCl_4 with ascorbic acid using cetyltrimethylammonium chloride as surfactant [90]. The third route is to introduce specific metal ions that can facilitate the alloying process. Xie and co-workers presented a facile method for the preparation of hexoctahedral Au—Pd alloyed nanocrystals with assistance of Cu^{2+} ions [91]. The underpotential deposition of Cu on Au was employed as a bridge to improve the alloying of Pd into a Au lattice. The comparative experiment confirmed that phase separation would occur in the absence of Cu^{2+} ions.

Recently, an effective general and convenient strategy for the synthesis of a large variety of alloyed nanocrystals with well controlled composition, size, and morphology has been developed by our group [92,93]. In our synthetic system, octadecylamine (ODA) was selected to serve simultaneously as solvent, surfactant and reducing agent. When noble-metal ions (Au^{3+}, Pd^{2+}, Pt^{4+}, Ir^{3+}, Ru^{3+}, Rh^{3+}, etc.) and non-noble metal ions (Fe^{3+}, Co^{2+}, Ni^{2+}, Cu^{2+}, Zn^{2+}, Cd^{2+}, In^{3+}, Sn^{2+}, etc.) coexisted in this system, alloys of noble and non-noble metals could be obtained under controlled conditions. That is, noble and non-noble metal ions can be co-reduced by ODA. This is a surprising and ingenious chemical process. As we know, ODA has weak reducing power at high temperature [94], and it can only reduce noble-metal ions [95]. When non-noble metal inorganic salts were added solely into ODA solvent at high temperature, corresponding metal oxides were products [96]. However, non-noble metal ions can be reduced in the presence of noble-metal ions in ODA system. It seems that noble metals (first reduced by ODA) can reduce non-noble metal ions, which is opposite to the classic galvanic theory. This phenomenon was also observed by some other researchers [97,98]. Murray and co-workers demonstrated that Ag^+ ions could be reduced by Au nanocluster [97]. Wu also revealed that approximately 2 and 3 nm sized Au nanoparticles could react with Ag^+ ions, and approximately 3 nm sized Ag nanoparticles could react with Cu^{2+} ions [98]. This novel chemical process can be named as anti-galvanic reduction, which could provide a facile and powerful route to prepare alloys on the nanoscale. Fig. 9 shows the typical TEM images of $InPt_3$, $CdPt_3$, CuPt, and CuPd nanocrystals, from which we can see that our developed method is effective to make high-quality alloyed nanocrystals. We can easily tune the composition, size, and shape of alloys via control over the experimental conditions including reaction temperature, reaction time, the concentration of reactants, and the molar ratio of two metal precursors.

Alloyed nanocrystals can also be synthesized by gas-phase method which is absolutely different from liquid-phase approaches [99]. Although the gas-phase method usually requires complicated apparatus and the operation is complex, as a ''bottom—up'' approach, it starts from atomic-level precursors and has better control over nucleation and growth of nanocrystals. Very recently, Lin and Sankaran exploited a gas-phase method for the synthesis of multimetallic nanoparticles without use of any chemical reducing agents or surfactants [99]. In their process, vapors of organometallic compounds (e.g., bis(cyclopentadienyl)nickel [$Ni(Cp)_2$] and copper acetylacetonate [$Cu(acac)_2$] for NiCu alloys) were introduced into a direct current, atmospheric-pressure microplasma reactor,

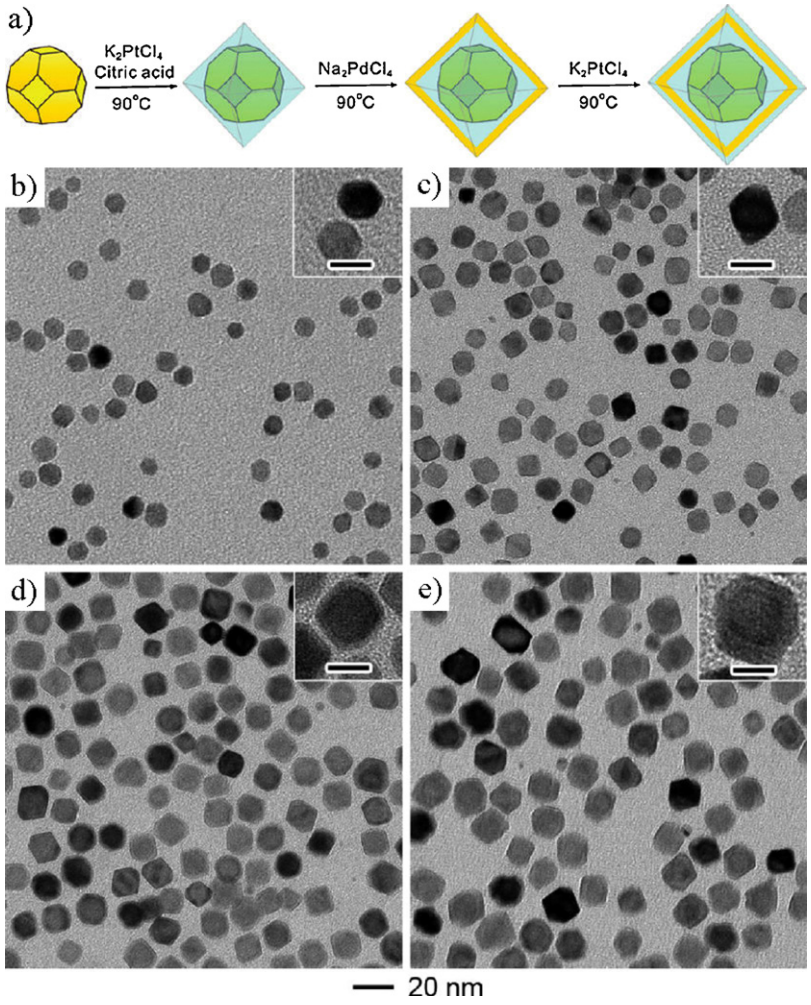

Figure 8 (a) Schematic illustration of producing multishelled nanocrystals; TEM images of (b) Pd, (c) Pd@Pt, (d) Pd@Pt@Pd, and (e) Pd@Pt@Pd@Pt nanocrystals. Insets: TEM images of individual nanocrystals at a higher magnification. Scale bars are 10 nm. Reproduced with permission from [84].

which were dissociated in a plasma volume to homogeneously nucleate particles (Fig. 10). By carefully combining precursor vapors and varying the flow rates, a wide range of compositionally controlled alloyed nanoparticles (less than 5 nm in diameter) with narrow size distributions can be prepared by this method.

Additionally, alloyed nanocrystals can emerge as one-dimensional morphology. In recent years, preparation of various monometallic nanowires and nanotubes has been achieved [100—102]. For example, single-crystalline Au nanowires were synthesized by the reduction of $HAuCl_4$ using oleylamine or other reducing agents [100,101]; ultrathin Pt nanowires were obtained with the assistance of chromium hexacarbonyl [$Cr(CO)_6$] [102]. However, design of synthetic system to obtain one-dimensional bimetallic nanostructures is much more complicated due to the different nucleation and growth process of two distinct metals [103—106]. Our group has made some progress in solution-based synthesis of ultrathin Au/Ag bimetallic nanowires [107]. Using $HAuCl_4{\cdot}4H_2O$ and $AgNO_3$ as the starting materials and octadecylamine as single solvent functioning simultaneously as surfactant and reducing agent, Au/Ag bimetallic nanowires with diameters of about 2 nm were synthesized (Fig. 11). The investigation of nucleation and growth process indicated that Au/Ag bimetallic ultrathin nanowires formed through the oriented attachment of primary nanoparticles and the wire—particle or wire—wire fusion. The key factors in determining the formation of nanowires from primary nanoparticles are the temperature and the composition of the nanoparticles. Nanowires can't be obtained for both Au and Ag rich alloy nanostructures, and a proper reaction temperature was found to be necessary for the formation of Au/Ag nanowires. This synthetic strategy and the underlying mechanism could be suggestive for the synthesis of other bimetallic nanowires.

Porous structure

Endowing bimetallic nanomaterials with high surface area is crucial for their catalytic applications. In the early years, the traditional metallurgical techniques produced alloys with very low surface area and thus low catalytic activity [108]. Although the developed nanotechnology can produce

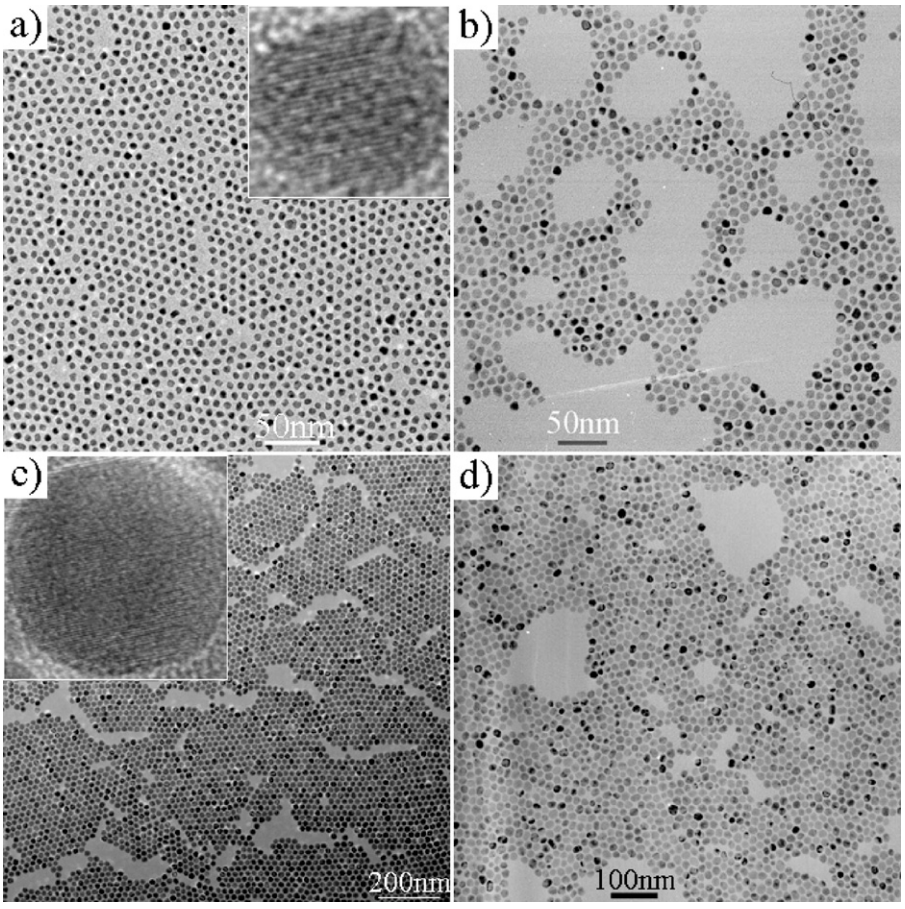

Figure 9 TEM images of (a) $InPt_3$, (b) $CdPt_3$, (c) CuPt, and (d) CuPd nanocrystals. Reproduced with permission from [92].

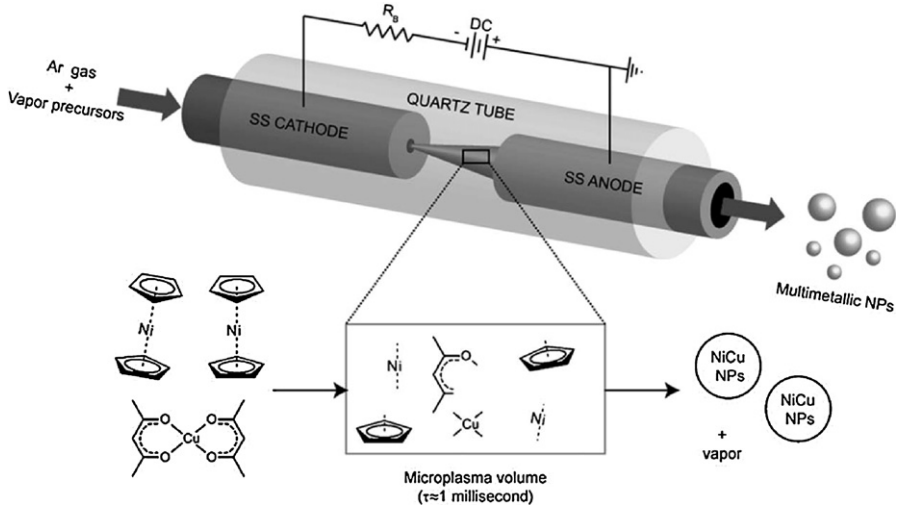

Figure 10 Schematic illustration of producing multimetallic nanoparticles via a gas-phase method. Reproduced with permission from [99].

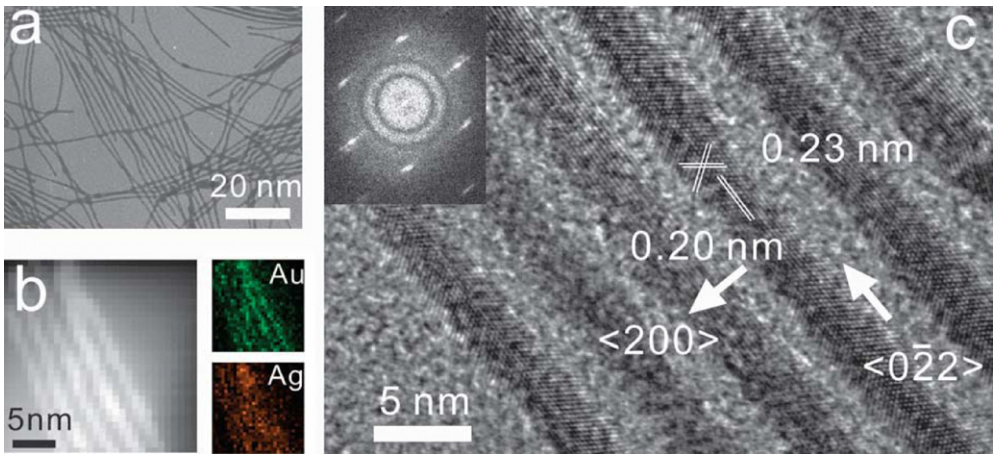

Figure 11 TEM (a), HAADF-STEM (high-angle annular dark-field scanning transmission electron microscopy) (b), and HRTEM (c) images of Au/Ag bimetallic nanowires.
Reproduced with permission from [107].

nanocrystalline alloys with small size and high surface area, alloys with larger surface area are still urgently desirable for the enhancement of catalytic properties. Porous structured alloys have the advantages of high surface area, high gas permeability, and low density, and therefore are more promising in catalytic applications than their solid counterparts. In 1927, American engineer Murray Raney produced porous nickel—aluminum alloy by selective leaching of a block of nickel—aluminum alloy with concentrated sodium hydroxide [109]. The well-known Raney nickel has been used as a heterogeneous catalyst for more than 80 years due to its high catalytic activity. In the following years, the chemical/electrochemical dealloying treatment which is the selective leaching of a less-noble metal from alloy precursor material has been developed to be an important method to make porous alloys [110—113]. Very recently, we exploited a facile chemical dealloying process to produce porous nanoparticles [114], that is, using nanocrystalline alloys as precursors, we selectively dissolve the less-noble component with an excess amount of concentrated nitric acid to leave a nanoporous residue. The developed procedure is a general strategy. Any nanocrystalline alloys of noble and non-noble metals can be effectively corroded via this route to produce corresponding nanoporous nanoparticles. Because the methodology to make nanocrystalline alloys has been well established in recent years, a large variety of alloy nanoporous nanoparticles can be prepared by dealloying alloyed nanocrystal precursors. Fig. 12a—d show the typical TEM images of Pt—Ni, Pt—Co, Pt—Cu, and Rh—Ni nanoporous nanoparticles respectively synthesized via our developed dealloying method. These nanoporous alloys possess some advantageous material properties including large surface area which can enhance the catalytic activity and small pores with a narrow pore-size distribution which can improve the catalytic selectivity. This chemical dealloying treatment with nanocrystalline alloys provides a universal, simple, and environmentally friendly synthetic route for nanoporous alloys with extraordinary structural characteristics.

Bimetallic porous nanostructures can also be synthesized by some other methods [115,116]. One of them is based on one-step process. De Hosson and co-workers reported a facile one-step synthetic route for bimetallic Au—Ag nanoparticles with porosity through their entire bulk [115]. In their process, presynthesized nanocrystalline AuAg alloys aren't required, which is different from the aforementioned dealloying method. The synthesis directly started from $HAuCl_4$ and $AgNO_3$ with the presence of a reducing agent (ethylene glycol) and a capping agent (PVP). To avoid the formation of solid Au—Ag nanoparticles, the processing conditions must be precisely controlled. Under the proper conditions, two processes of alloying between Ag and Au and galvanic replacement reaction between Ag and Au^{3+} ions occurred simultaneously and competed with each other, leading to the formation of porous bimetallic Au—Ag nanoparticles. Another commonly used method is based on templating approach. Kuroda and co-workers demonstrated the successful synthesis of mesoporous Pt—Au binary alloys using two-dimensional (2D) hexagonally ordered lyotropic liquid crystals (LLCs) as templates [116]. Fig. 13 systematically illustrates the preparation procedure which contains three steps. First, LLC templates containing corresponding metal species were prepared on conductive substrates. Then, Pt^{4+} and Au^{3+} ions were co-reduced via electrochemical depositions. Finally, the surfactants and undeposited metal species were removed by washing with ethanol and water. LLC templates play key roles in the synthesis. On one hand, they endow Pt—Au alloys with well-ordered 2D hexagonal mesostructures. On the other hand, they help Pt^{4+} and Au^{3+} ions to be uniformly co-reduced via interaction between metal ions and the ethylene oxide groups. In addition, by simply varying Au^{3+}/Pt^{4+} mole ratios, the composition of mesoporous Pt—Au alloys can be well controlled. The templating approach can also be applied to prepare one-dimensional bimetallic porous nanostructures [117—120]. Very recently, Yu and co-workers developed a general strategy for high-quality free-standing noble-metal (Pd, Pt, Au, Ag) sub-micron tubes composed of nanoparticles by a

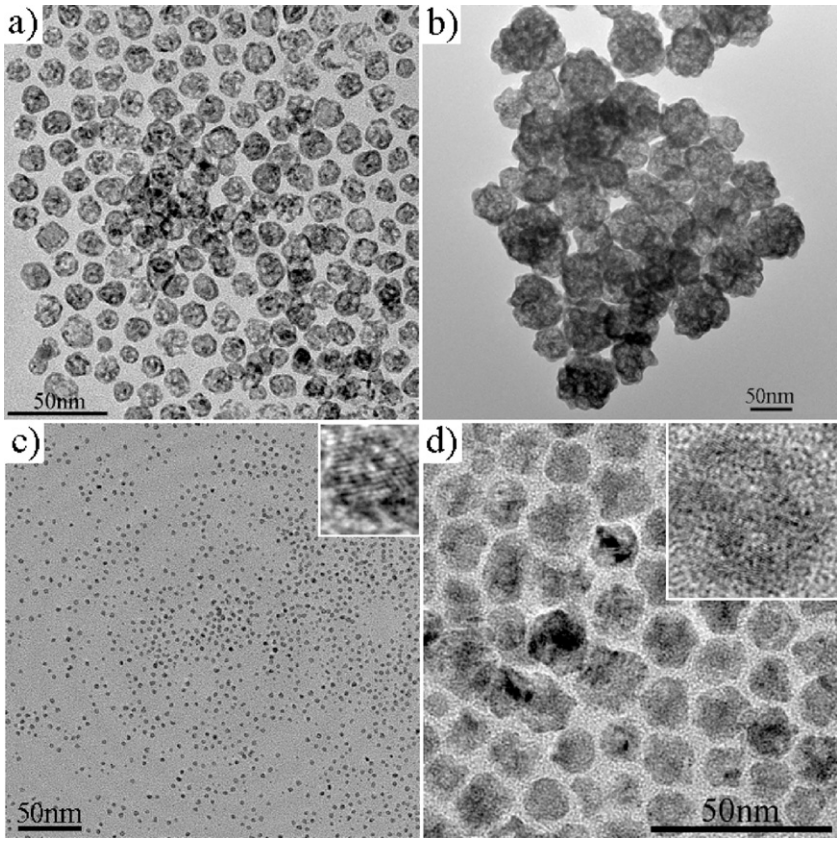

Figure 12 TEM images of (a) Pt—Ni, (b) Pt—Co, (c) Pt—Cu, and (d) Rh—Ni nanoporous nanoparticles. Reproduced with permission from [114].

one-step electrodeposition route onto an anodic aluminum oxide (AAO) template in anhydrous dimethyl sulfoxide (DMSO) solution [121]. This templating method was subsequently proved to be effective in preparing Pd—Au bimetallic nanoparticle tubes [117] and even ternary heterostructured nanoparticle tubes [118]. Fig. 14a shows scanning electron microscopy (SEM) image of Pd—Au bimetallic nanoparticle heterostructure tubes synthesized via the templating method. The transmission electron microscopy (TEM) image (Fig. 14b) indicates that the tube

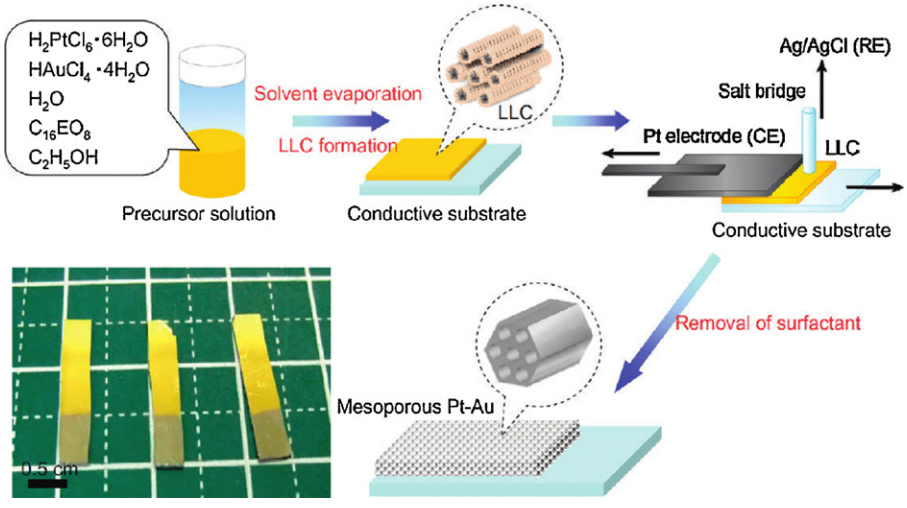

Figure 13 Schematic illustration of producing mesoporous Pt—Au binary alloys. Reproduced with permission from [116].

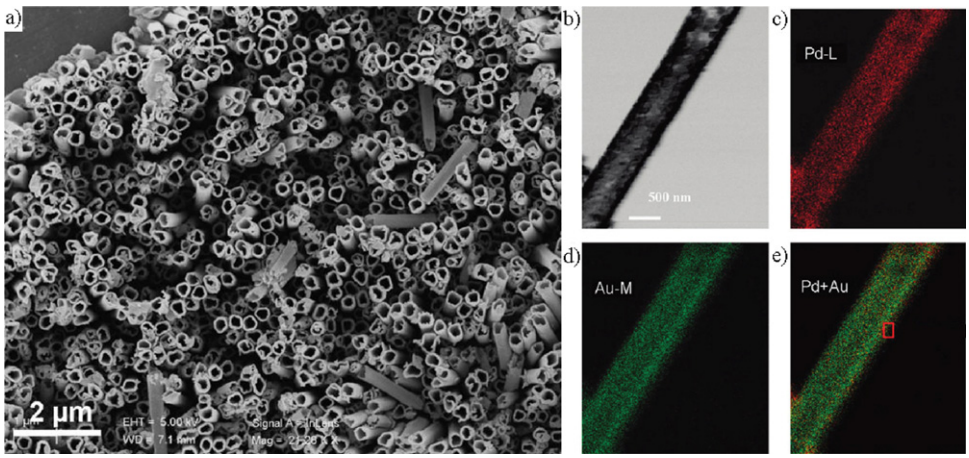

Figure 14 SEM (a) and TEM (b) images of Pd—Au bimetallic nanoparticle heterostructure tubes; (c—e) EDS mapping of Pd—Au tubes.
Reproduced with permission from [117].

wall is built by many flocky-like spheres, and these spheres consist of tiny nanocrystals. The energy-dispersive X-ray spectroscopy (EDS) mapping result reveals that the elements Au and Pd are uniformly dispersed in tubes (Fig. 14c—e). The as-obtained tubular bimetallic nanomaterials have a large surface area and highly active points for catalytic applications.

Generally speaking, the control over structures of bimetallic nanocrystals is achieved by tuning thermodynamic parameters (temperature, reduction potential, etc.) and kinetic parameters (reactant concentration, diffusion, solubility, reaction rate, etc.) during the synthetic procedures. When the parameters vary, the atomic distribution of two different metal atoms will change, leading to the transformation between different nanostructures. For example, with the increase of the injection rate of an aqueous $AgNO_3$ solution into the synthetic system, the structure of Pd—Ag bimetallic nanocrystals can change from heterostructure to core—shell structure [71]. We must note that, the transformation between different nanostructures is a common phenomenon, which usually occurs during application process. Since the catalytic properties of bimetallic nanomaterials are closely associated with their structures, the change in nanostructures must be considered during their catalytic application process.

Catalytic properties of bimetallic nanomaterials: key influencing factors

Structure effect

Compared to monometallic nanocatalysts, bimetallic nanomaterials show greater potential in catalytic applications due to their enhanced catalytic properties [122—125]. More importantly, nanocatalysts which consist of two distinct metals allow more flexible design according to the activity/selectivity requirements for a practical reaction. Herein, we discuss the structure effect for Pt-based bimetallic nanomaterials. As we know, Pt is the most active electrocatalyst for oxygen reduction reaction in proton-exchange membrane fuel cells. In order to improve the utilization of Pt, reduce Pt-loading in the catalysts, and increase the activity of catalysts, constructing bimetallic nanostructures consisting of Pt and some other metals is usually required. The addition of another metal to Pt can modify electronic properties of Pt and change Pt—Pt bond distance and coordination number of Pt, and consequently influence the catalytic properties of Pt. The atomic distribution between Pt and another metal plays a key role in determining performance of catalysts. There are generally several different ways to design Pt-based bimetallic nanostructures: (1) Pt islands supported on single-crystal metal substrates. Nilsson and co-workers investigated the anodic oxidation of Pt/Rh(1 1 1) and Pt/Au(1 1 1), and predicted that Pt/Rh(1 1 1) would show good long-term stability [126]. (2) Pt monolayer (ML) supported on another metal. Chen and co-workers demonstrated high activity of nanostructured Pt ML electrocatalyst for the hydrogen evolution reaction. The catalyst was fabricated by depositing one monolayer of Pt onto the faceted C/Re(1 1 2 1) surface [127]. (3) Core—shell structure with platinum-rich shell. Strasser et al. prepared Pt—Cu core—shell electrocatalyst with a pure Pt shell that surrounded a Pt—Cu alloy core [128]. This structure can modify the electronic band structure of Pt and weaken the adsorption energy of oxygenated species, leading to an increase in the catalytic activity for the oxygen reduction reaction. (4) Alloying Pt with another metal. Zhong and co-workers designed alloy electrocatalysts through alloying Pt with some transition metals and studied the correlation between atomic coordination structure and the electrocatalytic performance by treating the catalysts at different temperatures [129]. With increasing treatment temperature, the heteroatomic coordination number increased with improved alloying structure, resulting in enhanced Pt-alloying surface sites and consequently higher specific electrocatalytic activity. These Pt-based nanostructures possess their own structural characteristics

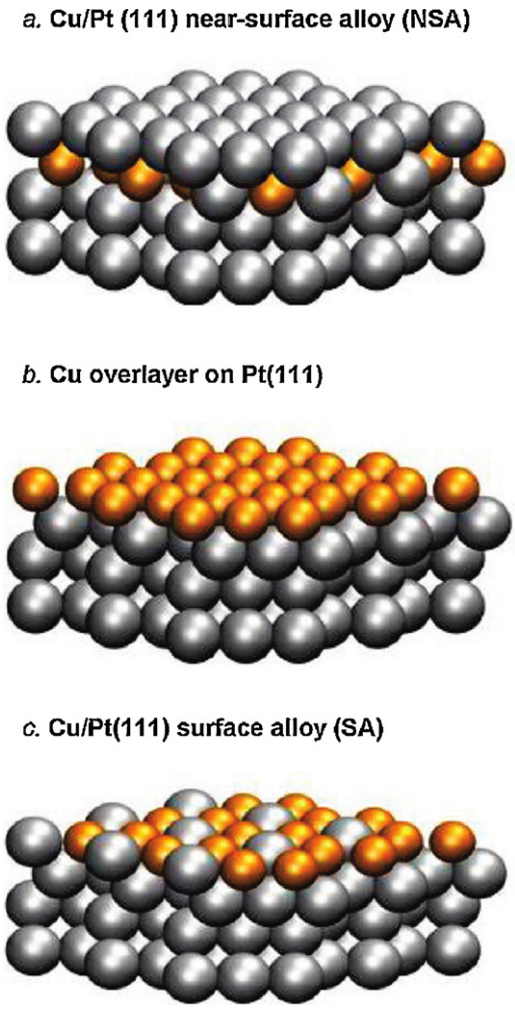

Figure 15 Schematic illustration of different ways of incorporating monolayer quantities of Cu into Pt(1 1 1).
Reproduced with permission from [130].

respectively and have different influence on the catalytic properties of Pt. Very recently, Chorkendorff and co-workers developed a subsurface alloying method to enhance the Pt activity for oxygen electroreduction and further confirmed the structure effect for Pt-based bimetallic nanomaterials [130]. Fig. 15 shows different ways of incorporating monolayer quantities of Cu into Pt(1 1 1). They are Cu/Pt(1 1 1) near-surface alloy (NSA), Cu overlayer on Pt(1 1 1), and Cu/Pt(1 1 1) surface alloy (SA) respectively. The experimental and theoretical studies have demonstrated that the binding of a Pt surface to intermediates in the ORR can be weakened in the presence of 3d metals (Cu). However, Cu will dissolve easily at high potentials once it reaches the surface. Therefore, Cu/Pt(1 1 1) NSAs represent the most optimal catalysts for ORR which result in an eight-fold enhancement in activity over Pt(1 1 1).

For other bimetallic nanomaterials, structure effect also plays a key role in determining their catalytic performance. Koel and co-workers investigated the relationship between the surface structures and ORR properties for bimetallic alloy single-crystal $Pd_3Fe(1\,1\,1)$ [131]. Density functional theory (DFT) calculations and some experimental results have confirmed that surface Fe has strong interaction with O_2 and is beneficial for oxygen dissociation, while monolayer Pd can lower the binding energy of oxygenated species to the surface and is helpful for fast removal of these species. Bimetallic alloys of Fe and Pd can combine the advantages of two metals. However, the surface atomic distribution of Fe and Pd can greatly influence their synergistic effect. In Pd—Fe alloys, Pd usually segregates to the topmost surface layer due to its lower surface energy. However, $Pd_3Fe(1\,1\,1)$ with surface free of Fe couldn't show high ORR activity. The heating treatment in ultrahigh vacuum was carried out to change the surface structure of $Pd_3Fe(1\,1\,1)$, and the results revealed that small amounts of Fe (approximately 10%) in the surface greatly enhanced ORR activity. The structure of bimetallic nanocrystals not only has great influence on the catalytic properties, but also can undergo reversible changes during catalytic reactions in some cases. Somorjai and co-workers proved the reaction-driven restructuring phenomenon of $Rh_{0.5}Pd_{0.5}$ core—shell nanoparticles [2]. The initial synthesized $Rh_{0.5}Pd_{0.5}$ nanoparticles have Rh-rich shell and Pd-rich core. Once placed in reducing environment, Pd would migrate to the shell while Rh would migrate to the core, leading to the formation of core—shell nanoparticles with Pd-rich shell. However, Rh would diffuse back to the shell when nanoparticles were placed in oxidizing environment. The atomic reorganization in reactive environments indicates the structural flexibility of bimetallic nanocrystals and a potential way to design bimetallic nanostructures based on the interplay of structure and reactivity.

Composition effect

Since the addition of another metal can change the properties of the primary metal, it is easy to understand that the molar ratio of two metals plays an important role in determining the catalytic performance of bimetallic nanomaterials [132—135]. For example, Lim and co-workers confirmed the composition-dependent activity of Pt—Y alloy catalysts for electrocatalytic oxygen reduction [136]. The addition of Y can change the electronic structure of Pt and thus modify the binding energy of the oxygen-containing species. Because the maximum possible catalytic activity can be achieved when the ability of Pt—Y alloy to bind the intermediates is medial, the activities of Pt-Y catalysts follow the trend of $Pt_{70}Y_{30} > Pt_{78}Y_{22} > Pt_{64}Y_{36} > Pt_{86}Y_{14} > Pt_{91}Y_9 > Pt$. Sun and co-workers proved the composition-dependent activity of monodisperse CoPd nanoparticles for catalytic formic acid oxidation [137]. Alloying Pd with Co is helpful for the absorption and activation of HCOOH. However, too much or too little Co in CoPd may not lead to a kinetically fastest catalytic reaction. Thus, the activities of CoPd nanoparticles decreased in the following sequence: $Co_{50}Pd_{50} > Co_{60}Pd_{40} > Co_{10}Pd_{90} > Pd$. The composition effect also exists in core—shell bimetallic nanoparticles. Xu and co-workers demonstrated the composition-dependent catalytic activity of Cu@M (M = Co, Fe, Ni) nanoparticles for hydrolytic dehydrogenation of ammonia borane [138]. In the Cu@M core—shell architectures, the interaction of Cu and M can change the width of surface d band, which is ben-

efit for the enhancement of catalytic performance. For all three series of catalysts, there is an optimum Cu/M ratio that shows the best catalytic activity.

Actually, the composition effect is closely related to the structure effect. For bimetallic nanocrystals, changing the molar ratio of two metals usually leads to the change of their structures, especially the atomic distribution of two species on the surface. Stamenkovic and co-workers investigated the influence of composition effect on the surface structure and electrocatalytic properties of monodisperse Pt_xNi_{1-x} nanoparticles [139]. When Pt—Ni alloyed nanoparticles were used as catalysts for the oxygen reduction reaction, the surface Ni would be dissolved due to the acidic electrolyte and potential cycling. Consequently, the nanoparticles suffered a structure transformation from uniform distribution of the two metals to Pt—Ni alloys with a Pt-rich surface layer. There was close correlation between the initial particle composition and the thickness of the Pt-skeleton layer. Generally, the thickness increased with increasing the Ni content. For instance, a Pt-rich layer with a thickness of about 0.5 nm was formed for PtNi, while the $PtNi_3$ particle showed Pt-skeleton structure with a thickness of above 1 nm. The particle central region could modify the electronic properties of surface Pt, which was dependent on the thickness of the Pt-skeleton layer. A medial thickness was required for Pt—Ni nanoparticles to show the best catalytic performance. Therefore, the mass activities of Pt—Ni alloy nanoparticles with various compositions for the ORR followed the trend of $PtNi > PtNi_2 > Pt_3Ni > PtNi_3$ (Fig. 16).

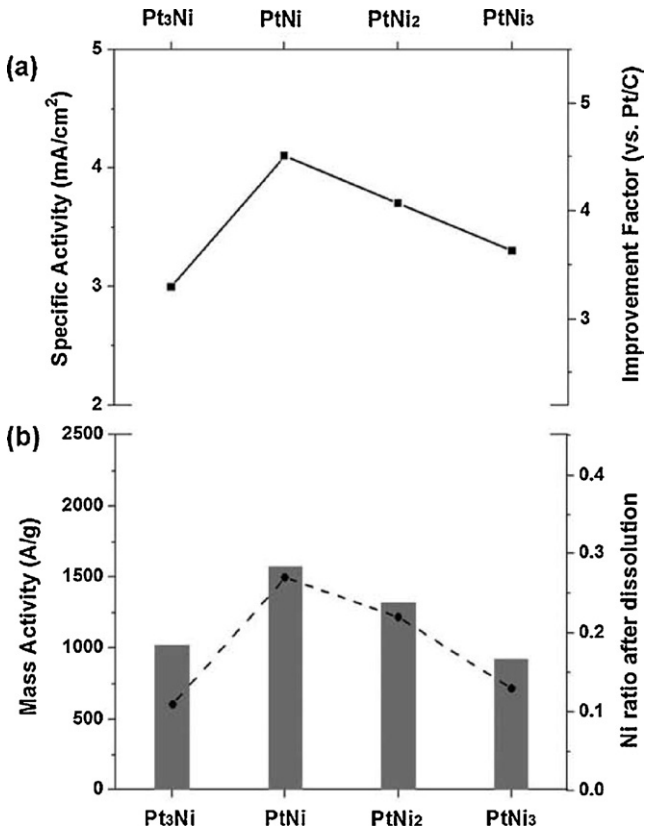

Figure 16 Comparison of (a) specific activities and (b) mass activities of Pt—Ni alloy nanoparticles with various compositions for the ORR.
Reproduced with permission from [139].

Size effect

For materials at the nanoscale, quantum-size effect is their basic characteristic. When particle size reduction takes place, the ratio of surface-to-volume increases and much more atoms are exposed on the surface. Consequently, novel physical and chemical properties that differ drastically from their bulk counterparts may emerge [140—142]. A classic example is Au: although Au in the bulk state is very unreactive, it shows high catalytic activity for low-temperature CO oxidation when the particle size is reduced to the nanometer scale [140]. The very recent investigation by Kitagawa and co-workers also revealed that Ir particles with nanosize of 1.5 ± 0.5 nm possessed hydrogen-storage capability, while Ir in the bulk form didn't absorb hydrogen absolutely [142]. The fascinating nanosize-induced properties of nanomaterials are size-dependent. Goodman and co-workers reported that Au nanoparticles with size of about 3.5 nm were the most active for the CO oxidation reaction [141]. The size of bimetallic nanocrystals also has decisive influence on their catalytic properties. However, size effect in bimetallic system is more complicated than that in monometallic system. For bimetallic nanoparticles, the change of size is usually accompanied by the change of atomic-scale structure. With the decrease of particle size, the distribution of two metals usually varies spontaneously to reduce the surface energy and produce the most thermodynamically stable mixing pattern. For example, Deng and co-workers have systematically investigated the segregation behavior and atomic-scale structure for Au—Ag bimetallic nanoparticles using Monte Carlo simulations [143]. They pointed out that, in smaller-sized nanoparticles, there were more obvious segregated features; while with the increase of particle size, the alloying extent was extended and the surface segregation was degraded.

The size-dependent catalytic properties of nanocrystalline bimetallic catalysts have been rarely reported. Sun and co-workers synthesized a series of monodisperse $Co_{60}Pd_{40}$ nanoparticles with controlled sizes ranging from 5 to 12 nm and studied the relationship between the particle size and their catalytic performance for formic acid oxidation [137]. Their preliminary results revealed that the 8 nm $Co_{60}Pd_{40}$ bimetallic nanocatalysts were more active than the 12 nm $Co_{60}Pd_{40}$ nanocatalysts and less active than the 5 nm $Co_{60}Pd_{40}$ nanocatalysts, that is, the catalytic activity of $Co_{60}Pd_{40}$ nanoparticles for formic acid oxidation increased with the decrease of particle size. Very recently, Somorjai and co-workers systemically investigated size effect of bimetallic $Rh_{0.5}Pt_{0.5}$ nanoparticle arrays in catalytic activity of CO oxidation and discussed the origin of the size effect [144]. A series of $Rh_{0.5}Pt_{0.5}$ binary nanoparticles with a size range between 5.7 and 11 nm were prepared via one-step polyol synthesis and used as nanocatalysts for CO oxidation. Fig. 17 illustrates the relationship between the turnover rate on bimetallic $Rh_{0.5}Pt_{0.5}$ nanoparticle arrays and their particle size. The results showed that $Rh_{0.5}Pt_{0.5}$ nanoparticles with smaller size possessed higher catalytic activity for CO oxidation compared to the bigger ones. X-ray photo-

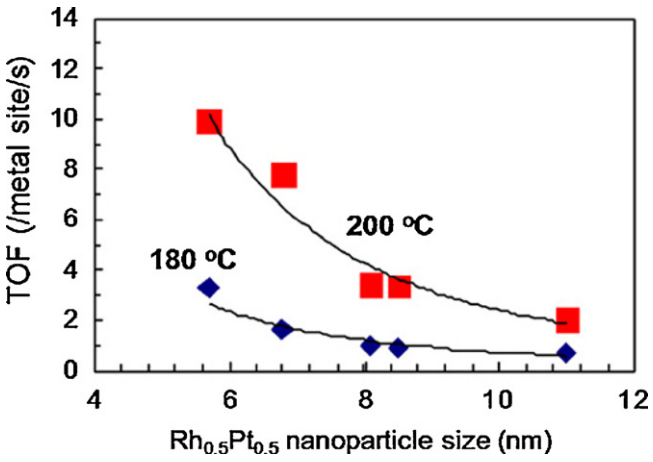

Figure 17 The relationship between the turnover rate on bimetallic $Rh_{0.5}Pt_{0.5}$ nanoparticle arrays and their particle size. Reproduced with permission from [144]. Copyright 2012 Elsevier.

electron spectroscopy (XPS) measurements revealed that, Rh was prone to segregate on the particle surface as the particle size decreased. The surface segregation of Rh led to the higher catalytic activity.

Morphology (crystal facet) effect

Since the catalytic reactions usually occur on the surface of catalysts, the exposed crystal facets of catalysts have significant influence on their catalytic performance, especially for structure-sensitive reactions. As early as 1981, Spencer et al., studied the catalytic activity of iron single crystals with well-defined crystal facets for ammonia synthesis [145]. The results indicated that iron with preferentially exposed (1 1 1) planes possessed the highest reaction rate, and the activity ratio for the (1 1 1), (1 0 0), and (1 1 0) planes was 418:25:1. For nanocrystals which are closer to the real catalytic systems, our group proved the shape-dependent catalytic properties on CeO_2 nanocrystals [146]. The results showed that CeO_2 nanorods predominantly exposing the well-defined (0 0 1) and (1 1 0) planes were more active than CeO_2 nanoparticles predominantly exposing the stable (1 1 1) planes for CO oxidation. Considering these points, in order to achieve designing a highly reactive/selective catalyst, the morphology of nanocrystals must be well controlled to expose more reactive crystal facets while less unreactive crystal facets. Therefore, for bimetallic nanocatalysts, it is very important to rationally control their particle shape to optimize the structure of active sites.

In the past few years, many groups have directed fundamental research focused on morphology (crystal facet) effect on the catalytic properties for bimetallic nanomaterials [7,12,147—150]. Hutchings and co-workers investigated the catalytic performance of supported Au—Pd alloy nanoparticles for the oxidation of primary carbon—hydrogen bonds [7]. There was a huge difference in catalytic activity between two catalysts (AuPd/C and AuPd/TiO_2), although both of them had a similar size distribution of Au—Pd nanoparticles. This difference related to the morphology and exposed crystal facets of the Au—Pd particles. In AuPd/C samples, most particles were icosahedral or decahedral which exclusively exposed (1 1 1) planes, while in AuPd/TiO_2 samples, most particles were cub-octahedral or single/double-twinned which exhibited mixed (1 0 0)/(1 1 1) facet terminations. The increasing proportion of (1 0 0) planes would lead to the decrease of catalytic activity. Yan and co-workers synthesized monodisperse single-crystalline (1 0 0) facet-enclosed Pt—Pd nanocubes and (1 1 1) facet-enclosed Pt—Pd nanotetrahedrons respectively and compared their catalytic properties (activity and durability) for methanol electrooxidations [147]. Due to the different reaction pathways on the (1 0 0) or (1 1 1) surfaces, Pt—Pd nanocubes exhibited a higher activity while Pt—Pd nanotetrahedrons possessed a better durability. Yang and co-workers prepared a series of Pt-based (Pt—M, M = Co, Fe, Ni, Pd) bimetallic nanocrystals with octahedral and cubic shapes, and studied their facet-dependent catalytic performances for ORR [12]. Fig. 18 shows the different electrocatalytic properties between cubic and octahedral Pt_3Ni nanocrystals. Because it has been demonstrated that the oxygen reduction activity on different Pt_3Ni crystal planes followed the trend of Pt_3Ni(1 1 1) > Pt_3Ni(1 1 0) Pt_3Ni(1 0 0), Pt_3Ni nanooctahedrons exposing (1 1 1) facets were more active than Pt_3Ni nanocubes exposing (1 0 0) facets.

Summary and perspective

In summary, this article highlights the recent progress in the synthesis of bimetallic nanomaterials with controllable architectures. Indeed, the synthetic techniques for bimetallic nanocrystals have been well developed in recent years. Various novel and creative strategies have been established and researchers can achieve easy control over structure, composition, size, and morphology of nanocrystals. However, most methods are empirical or semi-empirical. For most synthetic procedures, the underlying chemistry can't be fully understood. In other words, it is still a great challenge to understand the nucleation and growth mechanism of bimetallic nanocrystals. For instance, in the case of Au—Co nanoparticles obtained in the ODA synthetic system [82], it is difficult to understand the formation process. We proposed a noble-metal-induced-reduction mechanism, but frankly speaking, there was no direct evidence to explain how Au could induce the reduction of Co^{2+} ions. According to some clues, we supposed that, during the nucleation and growth process of Au, Au cluster which could reduce Co^{2+} ions formed. However, at present, the formation of cluster can't be confirmed and it is not clear exactly what happened during the process from mixed metal ions to Au—Co nanoparticles. Therefore, it is a very important issue to clarify the nucleation and growth mechanism of bimetallic nanocrystals. In the further work, researchers will focus their main attention on understanding the underlying chemistry and finding effective methods to achieve precise control over the nucleation and growth process of bimetallic nanocrystals.

We also discuss the relationship between the catalytic properties (e.g. activity, selectivity, and durability) of bimetallic nanoparticles with their structural characteristics in varied types of reactions. The key influencing factors including surface structure, composition, size, and morphology (crystal facet) have been investigated respectively by many groups. Although great progress has been made,

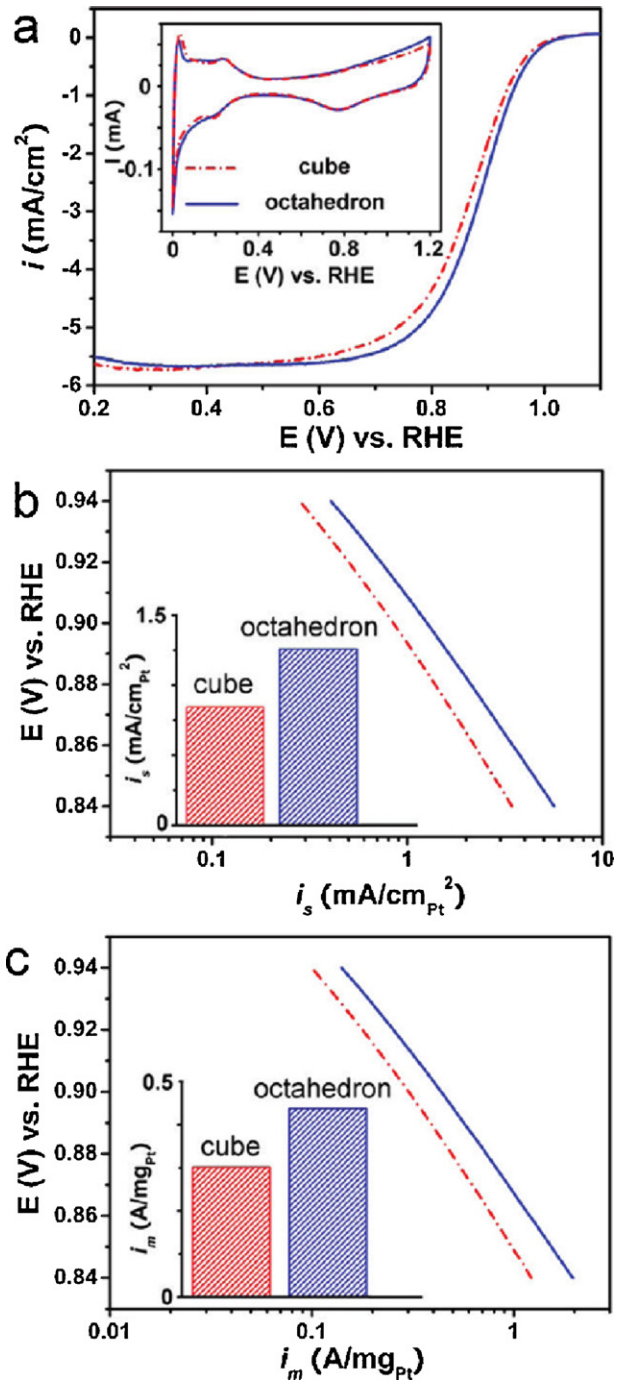

Figure 18 Comparison of electrocatalytic properties of cubic and octahedral Pt_3Ni nanocrystals.
Reproduced with permission from [12].
© 2011 American Chemical Society.

researchers still can't give satisfactory answers to some basic scientific issues: what kind of bimetallic nanocrystals probably possess the best catalytic performance for a given chemical reaction? What structural features are the most beneficial for the catalytic properties of bimetallic nanomaterials? How and why adding a second metal can change the chemical properties of the particles? Actually, in the field of nanocatalysis, there have been many basic problems puzzling the scientists. For example, why are Au nanoparticles with size of about 3.5 nm the most active for the CO oxidation reaction [141]? Similarly, for bimetallic catalysis, the catalytic mechanism can't be fully understood in most cases. In the case of $Co_{60}Pd_{40}$ nanocatalysts mentioned above [137], although the catalytic activity of the nanoparticles has been proven to increase with the decrease of particle size, it is not clear what will happen when the particle size is further reduced to a smaller scale (cluster). Therefore, based on exploring the correlation between microstructure and catalytic properties of bimetallic nanocrystals, researchers will deeply study the surface effect, quantum-size effect and interface effect at the nanoscale and fully understand the mechanism of catalytic reactions. In addition, as previously discussed, the transformation between different nanostructures usually occurs during application process. For bimetallic nanomaterials, surface segregation is an important phenomenon. For instance, alloyed nanocrystals might change to core—shell nanostructures during their catalytic application process [139]. Although the studies over surface segregation of bimetallic nanomaterials are challenging, it is believed that atomic-level understanding of structure—property correlation can be achieved by in situ microscopy techniques in the near future.

In a word, bimetallic nanocrystals, as a new class of materials, have great potential in catalytic applications. In this promising field, both basic theory and practical application have huge space for development. On one hand, researchers are very interested in thoroughly understanding some basic scientific issues in two aspects. Firstly, it is essential to realize how materials evolve from atoms to particles in order to achieve precise control over this process. Understanding the nucleation and growth mechanism of bimetallic nanocrystals can help us design and synthesize what we want. Secondly, in order to design more effective catalysts, it is necessary to reveal the synergy effects between two metals and make clear the most important factors that determine their properties. Understanding the catalytic mechanism of bimetallic nanocrystals can help us know what we need. On the other hand, the ultimate goal in this field is to achieve industrial applications of bimetallic nanocatalysts. In order to replace or partially replace the traditional industrial noble-metal catalysts (Pd/C, Pt/C, etc.), researchers are doing their best to develop new bimetallic nanocatalysts by rationally designing novel nanostructures and explore new catalytic reactions on the basis of thermodynamic and kinetic studies over the reaction process. It is believed that, in the following decade, exciting progress would be made in catalytic applications of bimetallic nanomaterials in various industrial catalytic reactions.

Acknowledgments

This work was supported by the State Key Project of Fundamental Research for Nanoscience and Nanotechnology (2011CB932401 and 2011CBA00500) and the National Natural Science Foundation of China (Grant Nos. 20921001 and 21131004).

References

[1] V.R. Stamenkovic, B. Fowler, B.S. Mun, G. Wang, P.N. Ross, C.A. Lucas, N.M. Markovic, Science 315 (2007) 493.
[2] F. Tao, M.E. Grass, Y. Zhang, D.R. Butcher, J.R. Renzas, Z. Liu, J.Y. Chung, B.S. Mun, M. Salmeron, G.A. Somorjai, Science 322 (2008) 932.
[3] B. Lim, M. Jiang, P.H.C. Camargo, E.C. Cho, J. Tao, X. Lu, Y. Zhu, Y. Xia, Science 324 (2009) 1302.
[4] T. Omori, K. Ando, M. Okano, X. Xu, Y. Tanaka, I. Ohnuma, R. Kainuma, K. Ishida, Science 333 (2011) 68.
[5] E. González, J. Arbiol, V.F. Puntes, Science 334 (2011) 1377.
[6] M. Chen, D. Kumar, C.W. Yi, D.W. Goodman, Science 310 (2005) 291.
[7] L. Kesavan, R. Tiruvalam, M.H. Ab Rahim, M.I. bin Saiman, D.I. Enache, R.L. Jenkins, N. Dimitratos, J.A. Lopez-Sanchez, S.H. Taylor, D.W. Knight, C.J. Kiely, G.J. Hutchings, Science 331 (2011) 195.
[8] G. Kyriakou, M.B. Boucher, A.D. Jewell, E.A. Lewis, T.J. Lawton, A.E. Baber, H.L. Tierney, M. Flytzani-Stephanopoulos, E.C.H. Sykes, Science 335 (2012) 1209.
[9] J.W. Hong, D. Kim, Y.W. Lee, M. Kim, S.W. Kang, S.W. Han, Angew. Chem. Int. Ed. 50 (2011) 8876.
[10] S. Habas, H. Lee, V. Radmilovic, G.A. Somorjai, P. Yang, Nat. Mater. 6 (2007) 692.
[11] Y. Yu, Q. Zhang, B. Liu, J.Y. Lee, J. Am. Chem. Soc. 132 (2010) 18258.
[12] J. Wu, A. Gross, H. Yang, Nano Lett. 11 (2011) 798.
[13] I. Nakamula, Y. Yamanoi, T. Imaoka, K. Yamamoto, H. Nishihara, Angew. Chem. Int. Ed. 50 (2011) 5830.
[14] M. McEachran, D. Keogh, B. Pietrobon, N. Cathcart, I. Gourevich, N. Coombs, V. Kitaev, J. Am. Chem. Soc. 133 (2011) 8066.
[15] B. Wickman, Y.E. Seidel, Z. Jusys, B. Kasemo, R.J. Behm, ACS Nano 5 (2011) 2547.
[16] G. Barcaro, A. Fortunelli, M. Polak, L. Rubinovich, Nano Lett. 11 (2011) 1766.
[17] Y. Kang, L. Qi, M. Li, R.E. Diaz, D. Su, R.R. Adzic, E. Stach, J. Li, C.B. Murray, ACS Nano 6 (2012) 2818.
[18] B. Lim, Y. Xia, Angew. Chem. Int. Ed. 50 (2011) 76.
[19] S. Guo, E. Wang, Nano Today 6 (2011) 240.
[20] W. Niu, G. Xu, Nano Today 6 (2011) 265.
[21] B. Wu, Y. Kuang, X. Zhang, J. Chen, Nano Today 6 (2011) 75.
[22] K. Cheng, S. Sun, Nano Today 5 (2010) 183.
[23] Q. Zhang, W. Wang, J. Goebl, Y. Yin, Nano Today 4 (2009) 494.
[24] K. An, T. Hyeon, Nano Today 4 (2009) 359.
[25] Z. Peng, H. Yang, Nano Today 4 (2009) 143.
[26] U. Banin, Nat. Mater. 6 (2007) 625.
[27] R. Hao, R. Xing, Z. Xu, Y. Hou, S. Gao, S. Sun, Adv. Mater. 22 (2010) 2729.
[28] X.L. Ji, K.T. Lee, R. Holden, L. Zhang, J.J. Zhang, G.A. Botton, M. Couillard, L.F. Nazar, Nat. Chem. 2 (2010) 286.
[29] Y.J. Kang, C.B. Murray, J. Am. Chem. Soc. 132 (2010) 7568.
[30] C. Wang, M. Chi, D. Li, D. Strmcnik, D. van der Vliet, G. Wang, V. Komanicky, K. Chang, A. Pauliks, D. Tripkovic, J. Pearson, K. More, N. Markovic, V. Stamenkovic, J. Am. Chem. Soc. 133 (2011) 14396.
[31] M. Oezaslan, M. Heggen, P. Strasser, J. Am. Chem. Soc. 134 (2012) 514.
[32] A.X. Yin, X.Q. Min, W. Zhu, H.S. Wu, Y.W. Zhang, C.H. Yan, Chem. Commun. 48 (2012) 543.
[33] B.H. Wu, H.Q. Huang, J. Yang, N.F. Zheng, G. Fu, Angew. Chem. Int. Ed. 51 (2012) 3440.
[34] S. Zhang, S.J. Guo, H.Y. Zhu, D. Su, S.H. Sun, J. Am. Chem. Soc. 134 (2012) 5060.
[35] M.S. Jin, H. Zhang, J.G. Wang, X.L. Zhong, N. Lu, Z.Y. Li, Z.X. Xie, M.J. Kim, Y.N. Xia, ACS Nano 6 (2012) 2566.
[36] Z.H. Lu, H.L. Jiang, M. Yadav, K. Aranishi, Q. Xu, J. Mater. Chem. 22 (2012) 5065.
[37] J. Snyder, I. McCue, K. Livi, J. Erlebacher, J. Am. Chem. Soc. 134 (2012) 8633.
[38] E. Panfilova, A. Shirokov, B. Khlebtsov, L. Matora, N. Khlebtsov, Nano Res. 5 (2012) 124.
[39] Z.C. Xu, E.C. Lai, S.H. Yang, K. Hamad-Schifferli, Chem. Commun. 48 (2012) 5626.
[40] D.S. Wang, Y.D. Li, Adv. Mater. 23 (2011) 1044.
[41] P. Venkatesan, J. Santhanalakshmi, Langmuir 26 (2010) 12225.
[42] V. Mazumder, M. Chi, K.L. More, S. Sun, J. Am. Chem. Soc. 132 (2010) 7848.
[43] F.R. Fan, D.Y. Liu, Y.F. Wu, S. Duan, Z.X. Xie, Z.Y. Jiang, Z.Q. Tian, J. Am. Chem. Soc. 130 (2008) 6949.
[44] P.P. Fang, S. Duan, X.D. Lin, J.R. Anema, J.F. Li, O. Buriez, Y. Ding, F.R. Fan, D.Y. Wu, B. Ren, Z.L. Wang, C. Amatore, Z.Q. Tian, Chem. Sci. 2 (2011) 531.
[45] F. Wang, C.H. Li, L.D. Sun, H.S. Wu, T.A. Ming, J.F. Wang, J.C. Yu, C.H. Yan, J. Am. Chem. Soc. 133 (2011) 1106.
[46] Y.J. Deng, N. Tian, Z.Y. Zhou, R. Huang, Z.L. Liu, J. Xiao, S.G. Sun, Chem. Sci. 3 (2012) 1157.
[47] X.Q. Huang, H.H. Zhang, C.Y. Guo, Z.Y. Zhou, N.F. Zheng, Angew. Chem. Int. Ed. 48 (2009) 4808.
[48] J.W. Hong, S.W. Kang, B.S. Choi, D. Kim, S.B. Lee, S.W. Han, ACS Nano 6 (2012) 2410.
[49] P.H.C. Camargo, Y.J. Xiong, L. Ji, J.M. Zuo, Y.N. Xia, J. Am. Chem. Soc. 129 (2007) 15452.
[50] X.Q. Huang, N.F. Zheng, J. Am. Chem. Soc. 131 (2009) 4602.
[51] H.L. Jiang, Q. Xu, J. Mater. Chem. 21 (2011) 13705.
[52] H. Zhang, T. Watanabe, M. Okumura, M. Haruta, N. Toshima, Nat. Mater. 11 (2012) 49.
[53] X.W. Lou, L.A. Archer, Z. Yang, Adv. Mater. 20 (2008) 3987.
[54] H. Zhang, M. Jin, H. Liu, J. Wang, M.J. Kim, D. Yang, Z. Xie, J. Liu, Y. Xia, ACS Nano 5 (2011) 8212.
[55] J.X. Wang, C. Ma, Y.M. Choi, D. Su, Y. Zhu, P. Liu, R. Si, M.B. Vukmirovic, Y. Zhang, R.R. Adzic, J. Am. Chem. Soc. 133 (2011) 13551.
[56] H. Wu, P. Wang, H. He, Y. Jin, Nano Res. 5 (2012) 135.
[57] L. Yang, C. Hu, J. Wang, Z. Yang, Y. Guo, Z. Bai, K. Wang, Chem. Commun. 47 (2011) 8581.
[58] X. Yu, D. Wang, Q. Peng, Y. Li, Chem. Commun. 47 (2011) 8094.
[59] X. Liu, X. Li, D. Wang, R. Yu, Y. Cui, Q. Peng, Y. Li, Chem. Commun. 48 (2012) 1683.
[60] K.M. Yeo, S. Choi, R.M. Anisur, J. Kim, I.S. Lee, Angew. Chem. Int. Ed. 50 (2011) 745.
[61] L. Wang, Y. Nemoto, Y. Yamauchi, J. Am. Chem. Soc. 133 (2011) 9674.
[62] B. Lim, M. Jiang, T. Yu, P.H.C. Camargo, Y. Xia, Nano Res. 3 (2010) 69.
[63] X. Liu, X. Liu, Angew. Chem. Int. Ed. 51 (2012) 3311.
[64] G. Krylova, L.J. Giovanetti, F.G. Requejo, N.M. Dimitrijevic, A. Prakapenka, E.V. Shevchenko, J. Am. Chem. Soc. 134 (2012) 4384.
[65] M.R. Buck, J.F. Bondi, R.E. Schaak, Nat. Chem. 4 (2012) 37.
[66] Z. Peng, H. Yang, Nano Res. 2 (2009) 406.
[67] Z. Peng, H. Yang, J. Am. Chem. Soc. 131 (2009) 7542.
[68] H. Lee, S.E. Habas, G.A. Somorjai, P. Yang, J. Am. Chem. Soc. 130 (2008) 5406.
[69] B. Lim, H. Kobayashi, T. Yu, J. Wang, M.J. Kim, Z.Y. Li, M. Rycenga, Y. Xia, J. Am. Chem. Soc. 132 (2010) 2506.
[70] J.H. Lee, G.H. Kim, J.M. Nam, J. Am. Chem. Soc. 134 (2012) 5456.
[71] J. Zeng, C. Zhu, J. Tao, M. Jin, H. Zhang, Z.Y. Li, Y. Zhu, Y. Xia, Angew. Chem. Int. Ed. 51 (2012) 2354.
[72] H.L. Jiang, T. Akita, T. Ishida, M. Haruta, Q. Xu, J. Am. Chem. Soc. 133 (2011) 1304.

[73] C. Wang, D. van der Vliet, K.L. More, N.J. Zaluzec, S. Peng, S. Sun, H. Daimon, G. Wang, J. Greeley, J. Pearson, A.P. Paulikas, G. Karapetrov, D. Strmcnik, N.M. Markovic, V.R. Stamenkovic, Nano Lett. 11 (2011) 919.
[74] Y.C. Wei, C.W. Liu, K.W. Wang, Chem. Commun. 47 (2011) 11927.
[75] G. Chen, S. Desinan, R. Nechache, R. Rosei, F. Rosei, D. Ma, Chem. Commun. 47 (2011) 6308.
[76] A. Alonso, N. Vigues, X. Munoz-Berbel, J. Macanas, M. Munoz, J. Mas, D.N. Muraviev, Chem. Commun. 47 (2011) 10464.
[77] X. Huang, S. Tang, B. Liu, B. Ren, N. Zheng, Adv. Mater. 23 (2011) 3420.
[78] D. Kim, Y.W. Lee, S.B. Lee, S.W. Han, Angew. Chem. Int. Ed. 51 (2012) 159.
[79] J. Xu, A.R. Wilson, A.R. Rathmell, J. Howe, M. Chi, B.J. Wiley, ACS Nano 5 (2011) 6119.
[80] F. Taufany, C.J. Pan, J. Rick, H.L. Chou, M.C. Tsai, B.J. Hwang, D.G. Liu, J.F. Lee, M.T. Tang, Y.C. Lee, C.I. Chen, ACS Nano 5 (2011) 9370.
[81] F. Yin, Z.W. Wang, R.E. Palmer, J. Am. Chem. Soc. 133 (2011) 10325.
[82] D.S. Wang, Y.D. Li, J. Am. Chem. Soc. 132 (2010) 6280.
[83] K. Aranishi, H.L. Jiang, T. Akita, M. Haruta, Q. Xu, Nano Res. 4 (2011) 1233.
[84] H. Zhang, M. Jin, J. Wang, M.J. Kim, D. Yang, Y. Xia, J. Am. Chem. Soc. 133 (2011) 10422.
[85] Y. Xu, S. Hou, Y. Liu, Y. Zhang, H. Wang, B. Zhang, Chem. Commun. 48 (2012) 2665.
[86] W.J. Yoo, H. Miyamura, S. Kobayashi, J. Am. Chem. Soc. 133 (2011) 3095.
[87] X. Gu, Z.H. Lu, H.L. Jiang, T. Akita, Q. Xu, J. Am. Chem. Soc. 133 (2011) 11822.
[88] S. Guo, S. Sun, J. Am. Chem. Soc. 134 (2012) 2492.
[89] S.K. Singh, A.K. Singh, K. Aranishi, Q. Xu, J. Am. Chem. Soc. 133 (2011) 19638.
[90] Y.W. Lee, M. Kim, S.W. Kang, S.W. Han, Angew. Chem. Int. Ed. 50 (2011) 3466.
[91] L. Zhang, J. Zhang, Q. Kuang, S. Xie, Z. Jiang, Z. Xie, L. Zheng, J. Am. Chem. Soc. 133 (2011) 17114.
[92] D.S. Wang, Q. Peng, Y.D. Li, Nano Res. 3 (2010) 574.
[93] D.S. Wang, Y.D. Li, Inorg. Chem. 50 (2011) 5196.
[94] H. Zheng, R.K. Smith, Y. Jun, C. Kisielowski, U. Dahmen, A.P. Alivisatos, Science 324 (2009) 1309.
[95] D.S. Wang, T. Xie, Q. Peng, Y.D. Li, J. Am. Chem. Soc. 130 (2008) 4016.
[96] D.S. Wang, T. Xie, Q. Peng, S.Y. Zhang, J. Chen, Y.D. Li, Chem. Eur. J. 14 (2008) 2507.
[97] J.P. Choi, C.A. Fields-Zinna, R.L. Stiles, R. Balasubramanian, A.D. Douglas, M.C. Crowe, R.W. Murray, J. Phys. Chem. C 114 (2010) 15890.
[98] Z. Wu, Angew. Chem. Int. Ed. 51 (2012) 2934.
[99] P.A. Lin, R.M. Sankaran, Angew. Chem. Int. Ed. 50 (2011) 10953.
[100] Z.Y. Huo, C.K. Tsung, W.Y. Huang, X.F. Zhang, P.D. Yang, Nano Lett. 8 (2008) 2041.
[101] X.M. Lu, M.S. Yavuz, H.Y. Tuan, B.A. Korgel, Y.N. Xia, J. Am. Chem. Soc. 130 (2008) 8900.
[102] Q. Xiao, M. Cai, M.P. Balogh, M.M. Tessema, Y. Lu, Nano Res. 5 (2012) 145.
[103] C. Zhu, S. Guo, S. Dong, Adv. Mater. 24 (2012) 2326.
[104] N.L. Netzer, C. Qiu, Y. Zhang, C. Lin, L. Zhang, H. Fong, C. Jiang, Chem. Commun. 47 (2011) 9606.
[105] S. Guo, S. Zhang, X. Sun, S. Sun, J. Am. Chem. Soc. 133 (2011) 15354.
[106] C.C. Mayorga-Martinez, M. Guix, R.E. Madrid, A. Merkoci, Chem. Commun. 48 (2012) 1686.
[107] X. Hong, D.S. Wang, R. Yu, H. Yan, Y. Sun, L. He, Z. Niu, Q. Peng, Y. Li, Chem. Commun. 47 (2011) 5160.
[108] C. Suryanarayana, Prog. Mater. Sci. 46 (2001) 1.
[109] M. Raney, U.S. Patent 1628190, (1927).
[110] J. Snyder, T. Fujita, M.W. Chen, J. Erlebacher, Nat. Mater. 9 (2010) 904.
[111] F.U. Renner, A. Stierle, H. Dosch, D.M. Kolb, T.L. Lee, J. Zegenhagen, Nature 439 (2006) 707.
[112] J. Rugolo, J. Erlebacher, K. Sieradzki, Nat. Mater. 5 (2006) 946.
[113] A. Pareek, S. Borodin, A. Bashir, G.N. Ankah, P. Keil, G.A. Eckstein, M. Rohwerder, M. Stratmann, Y. Grunder, F.U. Renner, J. Am. Chem. Soc. 133 (2011) 18264.
[114] D. Wang, P. Zhao, Y. Li, Sci. Rep. 1 (2011) 37, http://dx.doi.org/10.1038/srep00037.
[115] E. Detsi, S. Punzhin, P.R. Onck, J.Th.M. De Hosson, J. Mater. Chem. 22 (2012) 4588.
[116] Y. Yamauchi, A. Tonegawa, M. Komatsu, H. Wang, L. Wang, Y. Nemoto, N. Suzuki, K. Kuroda, J. Am. Chem. Soc. 134 (2012) 5100.
[117] C.H. Cui, J.W. Yu, H.H. Li, M.R. Gao, H.W. Liang, S.H. Yu, ACS Nano 5 (2011) 4211.
[118] C.H. Cui, H.H. Li, J.W. Yu, M.R. Gao, S.H. Yu, Angew. Chem. Int. Ed. 49 (2010) 9149.
[119] L. Liu, E. Pippel, Angew. Chem. Int. Ed. 50 (2011) 2729.
[120] C.H. Cui, H.H. Li, S.H. Yu, Chem. Sci. 2 (2011) 1611.
[121] C.H. Cui, H.H. Li, S.H. Yu, Chem. Commun. 46 (2010) 940.
[122] M.I. bin Saiman, G.L. Brett, R. Tiruvalam, M.M. Forde, K. Sharples, A. Thetford, R.L. Jenkins, N. Dimitratos, J.A. Lopez-Sanchez, D.M. Murphy, D. Bethell, D.J. Willock, S.H. Taylor, D.W. Knight, C.J. Kiely, G.J. Hutchings, Angew. Chem. Int. Ed. 51 (2012) 5981.
[123] J.S. Jirkovsk, I. Panas, E. Ahlberg, M. Halasa, S. Romani, D.J. Schiffrin, J. Am. Chem. Soc. 133 (2011) 19432.
[124] R. Mu, Q. Fu, H. Xu, H. Zhang, Y. Huang, Z. Jiang, S. Zhang, D. Tan, X. Bao, J. Am. Chem. Soc. 133 (2011) 1978.
[125] W. Yu, M.A. Barteau, J.G. Chen, J. Am. Chem. Soc. 133 (2011) 20528.
[126] D. Friebel, D.J. Miller, D. Nordlund, H. Ogasawara, A. Nilsson, Angew. Chem. Int. Ed. 50 (2011) 10190.
[127] X. Yang, B.E. Koel, H. Wang, W. Chen, R.A. Bartynski, ACS Nano 6 (2012) 1404.
[128] P. Strasser, S. Koh, T. Anniyev, J. Greeley, K. More, C. Yu, Z. Liu, S. Kaya, D. Nordlund, H. Ogasawara, M.F. Toney, A. Nilsson, Nat. Chem. 2 (2010) 454.
[129] B.N. Wanjala, B. Fang, J. Luo, Y. Chen, J. Yin, M.H. Engelhard, R. Loukrakpam, C.J. Zhong, J. Am. Chem. Soc. 133 (2011) 12714.
[130] I.E.L. Stephens, A.S. Bondarenko, F.J. Perez-Alonso, F. Calle-Vallejo, L. Bech, T.P. Johansson, A.K. Jepsen, R. Frydendal, B.P. Knudsen, J. Rossmeisl, I. Chorkendorff, J. Am. Chem. Soc. 133 (2011) 5485.
[131] X. Yang, J. Hu, J. Fu, R. Wu, B.E. Koel, Angew. Chem. Int. Ed. 50 (2011) 10182.
[132] H. Zhang, M. Jin, J. Wang, W. Li, P.H.C. Camargo, M.J. Kim, D. Yang, Z. Xie, Y. Xia, J. Am. Chem. Soc. 133 (2011) 6078.
[133] Y. Wu, D. Wang, P. Zhao, Z. Niu, Q. Peng, Y. Li, Inorg. Chem. 50 (2011) 2046.
[134] D. Sun, V. Mazumder, O. Metin, S. Sun, ACS Nano 5 (2011) 6458.
[135] M. Yin, Y. Huang, L. Liang, J. Liao, C. Liu, W. Xing, Chem. Commun. 47 (2011) 8172.
[136] S.J. Yoo, S.K. Kim, T.Y. Jeon, S.J. Hwang, J.G. Lee, S.C. Lee, K.S. Lee, Y.H. Cho, Y.E. Sung, T.H. Lim, Chem. Commun. 47 (2011) 11414.
[137] V. Mazumder, M. Chi, M.N. Mankin, Y. Liu, O. Metin, D. Sun, K.L. More, S. Sun, Nano Lett. 12 (2012) 1102.
[138] H.L. Jiang, T. Akita, Q. Xu, Chem. Commun. 47 (2011) 10999.

[139] C. Wang, M. Chi, G. Wang, D. van der Vliet, D. Li, K. More, H.H. Wang, J.A. Schlueter, N.M. Markovic, V.R. Stamenkovic, Adv. Funct. Mater. 21 (2011) 147.
[140] M. Haruta, N. Yamada, T. Kobayashi, S. Lijima, J. Catal. 115 (1989) 301.
[141] M. Valden, X. Lai, D.W. Goodman, Science 281 (1998) 1647.
[142] H. Kobayashi, M. Yamauchi, H. Kitagawa, J. Am. Chem. Soc. 134 (2012) 6893.
[143] L. Deng, W. Hu, H. Deng, S. Xiao, J. Tang, J. Phys. Chem. C 115 (2011) 11355.
[144] J.Y. Park, Y. Zhang, S.H. Joo, Y. Jung, G.A. Somorjai, Catal. Today 181 (2012) 133.
[145] N.D. Spencer, R.C. Schoonmaker, G.A. Somorjai, Nature 294 (1981) 643.
[146] K.B. Zhou, X. Wang, X.M. Sun, Q. Peng, Y.D. Li, J. Catal. 229 (2005) 206.
[147] A.X. Yin, X.Q. Min, Y.W. Zhang, C.H. Yan, J. Am. Chem. Soc. 133 (2011) 3816.
[148] J. Wu, H. Yang, Nano Res. 4 (2011) 72.
[149] K. Zhou, Y. Li, Angew. Chem. Int. Ed. 51 (2012) 602.
[150] Z. Niu, D. Wang, R. Yu, Q. Peng, Y. Li, Chem. Sci. 3 (2012) 1925.

Xiangwen Liu received his BS degree in Department of Chemistry, Shandong University in 2002, and his Master degree in College of Chemistry and Chemical Engineering, Graduate University of the Chinese Academy of Sciences in 2009. He joined Acad. Yadong Li's group as a PhD candidate in 2009.

Dingsheng Wang received his BS degree in Department of Chemistry and Physics, University of Science and Technology of China in 2004, and his PhD degree in Department of Chemistry, Tsinghua University in 2009, with Acad. Yadong Li. He did his postdoctoral research in Department of Physics, Tsinghua University, with Acad. Shoushan Fan. He joined the faculty of Department of Chemistry, Tsinghua University in 2012.

Yadong Li received his BS degree in Department of Chemistry, Anhui Normal University in 1986 and his PhD degree in Department of Chemistry, University of Science and Technology of China in 1998, with Acad. Yitai Qian. He joined the faculty of Department of Chemistry, Tsinghua University in 1999 as a full professor.